

Investigation of tourmaline characteristics in bedrock and surficial sediment samples from two Canadian porphyry copper systems

C.E. Beckett-Brown^{1*}, A.M. McDonald¹, M.B. McClenaghan²,
A. Plouffe², and T. Ferbey³

Beckett-Brown, C.E., McDonald, A.M., McClenaghan, M.B., Plouffe, A., and Ferbey, T., 2021. Investigation of tourmaline characteristics in bedrock and surficial sediment samples from two Canadian porphyry copper systems; in Targeted Geoscience Initiative 5: contributions to the understanding and exploration of porphyry deposits, (ed.) E. Schetselaar and A. Plouffe; Geological Survey of Canada, Bulletin 616, p. 109–135. <https://doi.org/10.4095/327989>

Abstract: Colour, texture, and chemistry were used to determine the source of tourmaline grains in local surficial (detrital) sediments from two Canadian porphyry systems (Woodjam and Casino). Tourmaline from porphyry bedrock is generally dark brown to black. Crystals frequently exhibit oscillatory and sector zoning, with overgrowth, irregular, and patchy patterns. Major-element analyses show ranges from schorl (Fe²⁺-rich; 0.04–3.07 *apfu*, av. 0.76) to dravite (Mg-rich, av. 2.00 *apfu*), with a minor povondraite (Fe³⁺) component. The alkali- and alkaline-earth element concentrations are relatively constant, with Na>Ca>□ and OH>O²⁻ dominant. Tourmaline in porphyry systems is characterized by high Cu (tens of parts per million) and Sr (hundreds of parts per million), and low Pb (<10 parts per million) and Zn (tens of parts per million). Detrital tourmaline occurs as euhedral grains and contains similar Fe and Mg concentrations and textural zonation patterns to porphyry tourmaline. Its trace-element content shows similarities but with larger ranges of values, likely related to the presence of non-porphyry detrital tourmaline. Overall, a combination of physical and chemical characteristics (oxy-dravite–povondraite trend, high Sr, low Zn and Pb) of tourmaline grains are useful in discriminating between porphyry- versus non-porphyry-derived (or related) tourmaline in both bedrock and surficial sediments.

Résumé : Nous avons utilisé les caractéristiques de couleur, de texture et de chimie pour déterminer la source des grains de tourmaline présents dans les sédiments superficiels (détritiques) locaux de deux systèmes porphyriques (Woodjam et Casino) au Canada. La tourmaline présente dans le substratum rocheux porphyrique exhibe une couleur qui varie généralement du brun foncé au noir. Les cristaux présentent fréquemment une zonation oscillatoire et sectorielle, avec des motifs d'accroissement secondaire, irréguliers et inégaux. Les analyses des éléments majeurs révèlent des plages de composition s'étendant du schorl (riche en Fe²⁺; de 0,04 à 3,07 atomes par unité de formule, moy. de 0,76) à la dravite (riche en Mg, moy. de 2,00 atomes par unité de formule), avec une composante mineure de povondraïte (Fe³⁺). Les concentrations d'éléments alcalins et alcalino-terreux sont relativement constantes, avec une dominance de Na>Ca>□ et de OH>O²⁻. La tourmaline dans les systèmes porphyriques est caractérisée par une teneur élevée en Cu (dizaines de parties par million) et en Sr (centaines de parties par million), et une faible teneur en Pb (<10 parties par million) et en Zn (dizaines de parties par million). La tourmaline détritique se présente sous forme de grains euhédriques et affiche des concentrations de Fe et de Mg et des motifs texturaux de zonation semblables à ceux de la tourmaline des systèmes porphyriques. Sa teneur en éléments en traces présente des similitudes, mais avec des fourchettes de valeurs plus larges, ce qui reflète probablement la présence de tourmaline détritique ne provenant pas de systèmes porphyriques. Dans l'ensemble, une combinaison de caractéristiques physiques et chimiques (tendance oxy-dravite–povondraïte, teneur élevée en Sr, faible teneur en Zn et Pb) des grains de tourmaline est utile pour distinguer la tourmaline de systèmes porphyriques de celle qui n'en provient pas (ou qui n'y est pas apparentée) dans le substratum rocheux et les sédiments superficiels.

¹Harquail School of Earth Sciences, Laurentian University, Willet Green Miller Centre, 935 Ramsey Lake Road, Sudbury, Ontario P3E 2C6

²Geological Survey of Canada, 601 Booth Street, Ottawa, Ontario K1A 0E8

³British Columbia Geological Survey, P.O. Box 9333, Stn Prov Gov't, Victoria, British Columbia V8W 9N3

*Corresponding author: C.E. Beckett-Brown (email: ce_beckettbrown@laurentian.ca)

INTRODUCTION

Exploration for new mineral deposits is becoming increasingly challenging as discovery rates decrease, expenditures increase, and exploration switches from surface-based methods to those that can detect buried deposits. Indicator mineral identification is one such technique that can detect mineral deposits buried beneath thick glacial sediment cover.

Recent studies have identified two groups of porphyry copper indicator minerals (Plouffe and Ferbey, 2017). Group 1 includes minerals that can be directly linked to porphyry copper mineralization based on their spatial distribution and abundance in surficial sediments (e.g. chalcopyrite, pyrite, gold, jarosite; Averill, 2011; Kelley et al., 2011; Hashmi et al., 2015; Plouffe et al., 2016; Plouffe and Ferbey, 2017). Group 2 includes minerals that are common in many geological environments but have specific chemical characteristics tied directly to mineralized porphyry systems, such as zircon (Lu et al., 2016), epidote (Cooke et al., 2014, 2017), apatite (Bouzari et al., 2016; Mao et al., 2016), titanite (Xu et al., 2015), and magnetite (Dare et al., 2014; Canil et al., 2017; Pisiak et al., 2017). Studies of indicator minerals typically focus either on those present in the bedrock environment (e.g. Cooke et al., 2014, 2017) or those found in surficial sediment such as till (Plouffe and Ferbey, 2017). This study combines multidimensional analyses of a specific supergroup of indicator minerals, tourmaline, derived from both bedrock and surficial (till and stream) sediments.

Several mineral groups have been evaluated as indicator minerals for mineralized porphyry systems (e.g. apatite, epidote, and chlorite group minerals; Wilkinson et al., 2017), but to date, the tourmaline supergroup has been overlooked. Tourmaline is a common constituent of many felsic rocks, notably pegmatites, but it is also common in the calc-alkaline to alkaline environments that characterize porphyry systems. Because of its colour, habit, and specific gravity, tourmaline can often be overlooked or mistaken for similar minerals (e.g. epidote, amphibole). Its hardness and resistance to chemical and physical weathering allow tourmaline to potentially serve as an effective indicator mineral. Tourmaline has proven extremely useful in other geological applications, including as a successful petrogenetic indicator mineral of its host rocks (Henry and Guidotti, 1985). The characteristics of tourmaline that make it an ideal long-term recorder of petrogenetic conditions include 1) the ability to accommodate a wide range of elements, 2) high hardness (7 on Mohs scale) and a lack of cleavage, and 3) insolubility under most terrestrial conditions. The overall long-term stability of tourmaline in the surficial environment also allows it to potentially record fluid evolution (including magmatic, magmatic-hydrothermal, and hydrothermal ore-forming fluids) during its crystallization history (Henry and Dutrow, 1996; Dutrow and Henry, 2011; Marschall and Jiang, 2011; van Hinsberg et al., 2011). In this sense, the growth history of a tourmaline crystal has the potential to record not only major features, but also subtle ones (e.g. trace-element

variations). Tourmaline should, therefore, closely reflect the chemical zonation that develops within a mineralized porphyry system.

Tourmaline is a common accessory mineral in hydrothermal deposits worldwide (Slack, 1996) and has been used to understand the development and evolution of select ore systems, including volcanogenic massive sulfide (VMS), orogenic gold, Sn-W, porphyry deposits and even emerald mineralization (Slack and Coad, 1989; Slack et al., 1993; Griffin et al., 1996; Frikken et al., 2005; Galbraith et al., 2009; Baksheev et al., 2010, 2011, 2012; Slack and Trumbull, 2011; Chapman et al., 2015; Codeço et al., 2017, 2019; Kalliomäki et al., 2017; Manégia et al., 2018).

The purpose of this study is to investigate and evaluate the applicability and usefulness of tourmaline as an indicator of mineralized porphyry copper systems. We focused on two sites, Woodjam in British Columbia and Casino in Yukon, examining tourmaline in the mineralized porphyry system (bedrock) as well as in local surficial sediments (stream sediments or till). This paper provides detailed documentation and comparisons of several key elements in tourmaline, including 1) chemical zonation and textural features, 2) major- and minor-element chemistry, and 3) trace-element chemistry. The comparison of tourmaline derived from the different media (i.e. surficial and bedrock) is crucial to the evaluation of the effectiveness of tourmaline as an indicator for porphyry deposits.

GEOLOGICAL BACKGROUND

Bedrock samples

The Casino deposit is a mineralized porphyry Cu-Mo-Au deposit located 300 km northwest of Whitehorse, Yukon. It is hosted in Late Cretaceous calc-alkalic quartz monzonite of the Casino suite (Casselman and Brown, 2017). Tourmaline is found throughout the deposit, including in breccias and veins, and as disseminations. Samples of all three textures of tourmaline were used in this study.

The Woodjam cluster is located in the Cariboo district, 50 km east of Williams Lake, British Columbia. Several types of mineralized porphyry systems hosted in Early Jurassic calc-alkaline intrusions (del Real et al., 2017) have been identified in the cluster: Megabuck and Deerhorn (Au-Cu), Southeast Zone (Cu-Mo), and Three Firs and Takom (Au-Cu). The tourmaline samples used in our study are from the Deerhorn and Takom deposits, where tourmaline occurs as an early alteration of the host rock, as disseminations, in breccias, and veins. The tourmaline investigated formed in a variety of alteration types, including 1) potassic, 2) phyllic, and 3) propylitic.

For comparison, we also analyzed tourmaline-bearing samples from other mineralized porphyry systems, including 1) Highland Valley Copper, British Columbia; 2) Schaft

Creek, British Columbia; 3) New Afton, British Columbia; and 4) Soledad, Peru. A suite of background tourmaline (i.e. non-porphyry) samples was also examined to provide a frame of reference for comparing tourmaline associated with mineralized porphyry systems to tourmaline not associated with mineralization. A complete listing of bedrock samples is presented in Table 2 of Beckett-Brown et al (2019).

Surficial samples

The Casino deposit is a deeply weathered porphyry that is largely intact due to minimal to no glacial erosion of the region during the past 2 million years (Godwin, 1976; Bond and Lipovsky, 2011). Bulk (10–15 kg) stream-sediment samples containing tourmaline were collected in 2017 from local first- and second-order streams (e.g. Casino Creek) located in narrow V-shaped valleys (Fig. 1b). Sampling details are reported in McCurdy et al. (2019) and McClenaghan et al. (this volume).

The Woodjam area is a glaciated landscape that was most recently affected by two phases of ice flow during the Late Wisconsin (Fraser glaciation; Clague and Ward, 2011): an older flow to the southwest and a younger flow to the northwest (Plouffe and Ferbey, 2016). As part of the TGI-4 program, the Geological Survey of Canada (GSC) and the British Columbia Geological Survey collected bulk (10–15 kg) till samples around the Woodjam cluster (during 2011–2013). Raw indicator mineral count data for the till samples, including those for tourmaline, were reported in Plouffe and Ferbey (2016). The samples were processed by Overburden Drilling Management (ODM) to produce mid-density (2.8–3.2 specific gravity (SG)) and heavy (>3.2 SG) mineral concentrates for counting indicator minerals in the 0.25 to 0.5 mm size fraction. Tourmaline abundance was reported as i) a percentage of the total heavy minerals in the greater than 3.2 SG fraction, ii) a percentage of the total minerals in the 2.8 to 3.2 SG fraction, and iii) a total number of grains in the 2.8 to 3.2 and greater than 3.2 SG fractions. Maps showing the distribution of tourmaline in till at Woodjam were presented by Chapman et al. (2015), and Plouffe and Ferbey (2017) plotted the number of grains in the 2.8 to 3.2 SG fraction normalized to 10 kg sample mass. In 2015, 50 tourmaline grains were removed from the 2.8 to 3.5 SG fraction of four of the till samples for mineral chemistry, the results of which are reported in Chapman et al. (2015).

The archived 2.8 to 3.2 SG and greater than 3.2 SG Woodjam concentrates were re-examined in 2016 by ODM as part of our current study. The original (2011–2013) tourmaline count data (Plouffe and Ferbey, 2016), the number of grains removed in 2015 for mineral chemistry, and the 2016 tourmaline recount data are summarized in Appendix A. There are important differences between the counts made in 2013 and 2016, specifically for the 2.8 to 3.2 SG fraction. The 2016 tourmaline grain count is more than 50% higher in 75 of 91 samples. It is difficult to visually

identify tourmaline in heavy mineral concentrates (HMC) based on its optical and physical properties; the differences in abundance show that the visual identification method can be highly subjective. Given that the 2016 recounts were specifically targeted at the identification of tourmaline and were completed by a senior mineralogist, we assert that the 2016 counts are more accurate. A new tourmaline abundance map for the 2.8 to 3.2 SG fraction of till based on the 2016 data is presented in Figure 1a.

METHODS

Sample processing

Surficial sediment samples (till and stream sediment) were collected by the GSC and processed by ODM to produce nonferromagnetic HMCs. Processing followed protocols outlined by Plouffe and Ferbey (2016) and McClenaghan et al. (2020). Tourmaline grains were primarily recovered in the sand-sized (0.25–2.0 mm), mid-density (2.8–3.2 SG) fraction of the surficial sediment samples, with minor amounts (approximately 1%) also recovered from the heavy (>3.2 SG) fraction. Tourmaline grains were visually identified by their dark brown colour, prismatic crystal habit, parallel striations on crystal faces, and conchoidal fracture (Fig. 2a). Selected grains were mounted in 2.5 cm epoxy pucks for imaging and chemical analysis. Grains were mounted perpendicular and parallel to the c-axis (elongation direction) to provide favourable orientations to examine any variations in chemical zonation with respect to the c-axis. Polished thin sections (PTS) of tourmaline-bearing bedrock samples were also prepared.

Major- and minor-element chemistry

Chemical analyses of major and minor elements in tourmaline grains in PTS and epoxy grain mounts were conducted by scanning electron microscopy–energy-dispersive spectroscopy (SEM-EDS) at Laurentian University on a JEOL 6400 SEM, with an accelerating voltage of 20 kV, a beam current of 1.0 nA, and 15 s counting times. Data were processed using INCA software. The primary standards were well characterized materials, including diopside (MgK α , CaK α , SiK α), albite (AlK α , NaK α), chalcopyrite (FeK α), and syn CaTiO₃ (TiK α). Representative chemical analyses are presented in Table 1. The chemical data were reduced to atoms per formula unit (*apfu*) based on 31 anions and this calculation was completed using WinTcac (Yavuz et al., 2011). Tourmaline ubiquitously exhibits zonation, typically about the c-axis, thus individual chemical zones were analyzed.

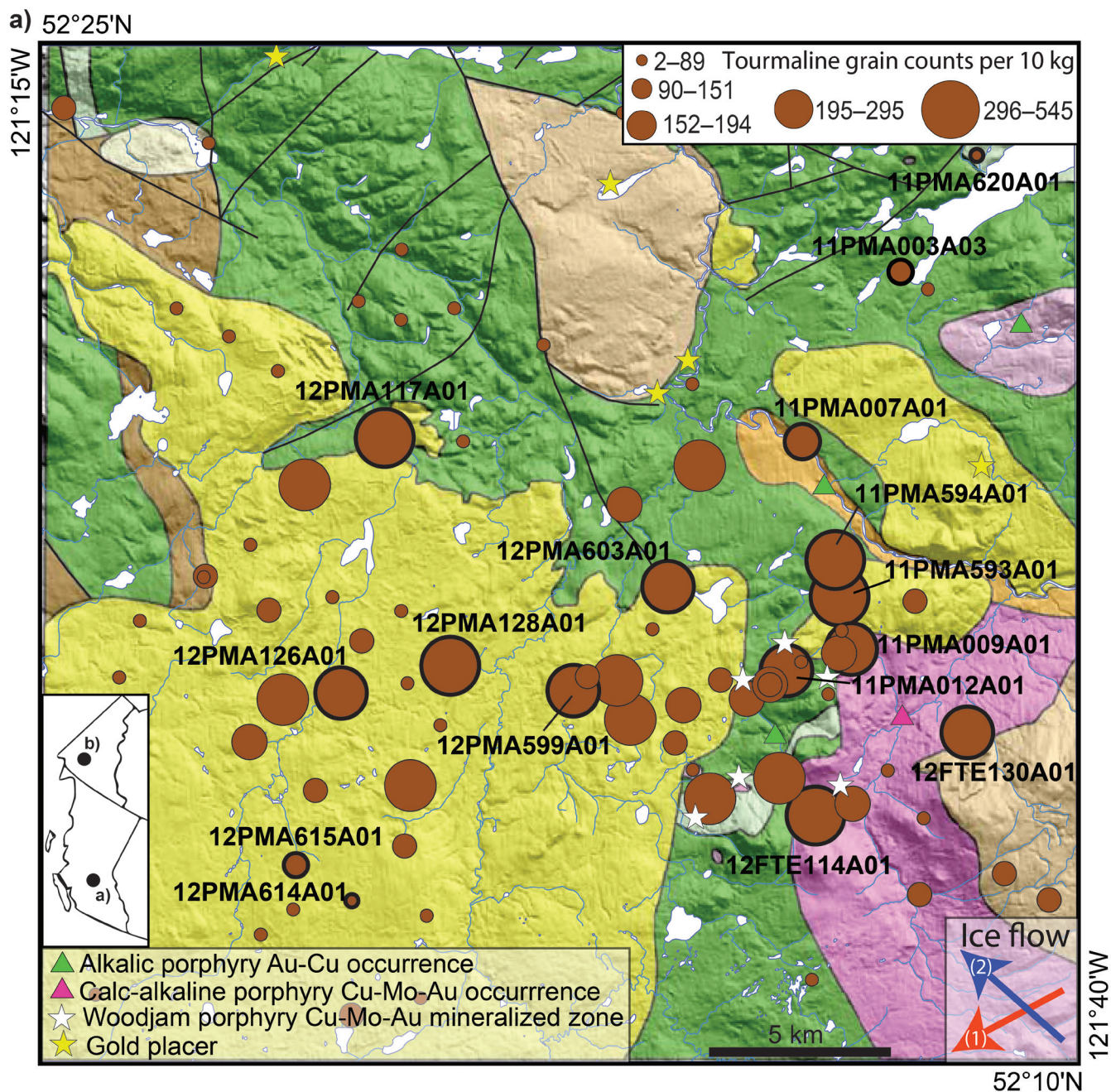


Figure 1. Location of surficial sediment samples from which tourmaline grains were recovered and examined in this study; inset map shows the location of **a)** the Woodjam deposit in British Columbia and **b)** the Casino deposit in Yukon: a) Proportional dot map of tourmaline abundance (grain counts, normalized to 10 kg) in the mid-density (2.8–3.2 SG) 0.25 to 0.5 mm fraction of till samples collected down ice of the Woodjam deposit cluster, British Columbia (unpublished Geological Survey of Canada data). See Plouffe and Ferbey (2017) for bedrock geology. Dots with the black outline indicate till samples from which tourmaline grains were investigated;

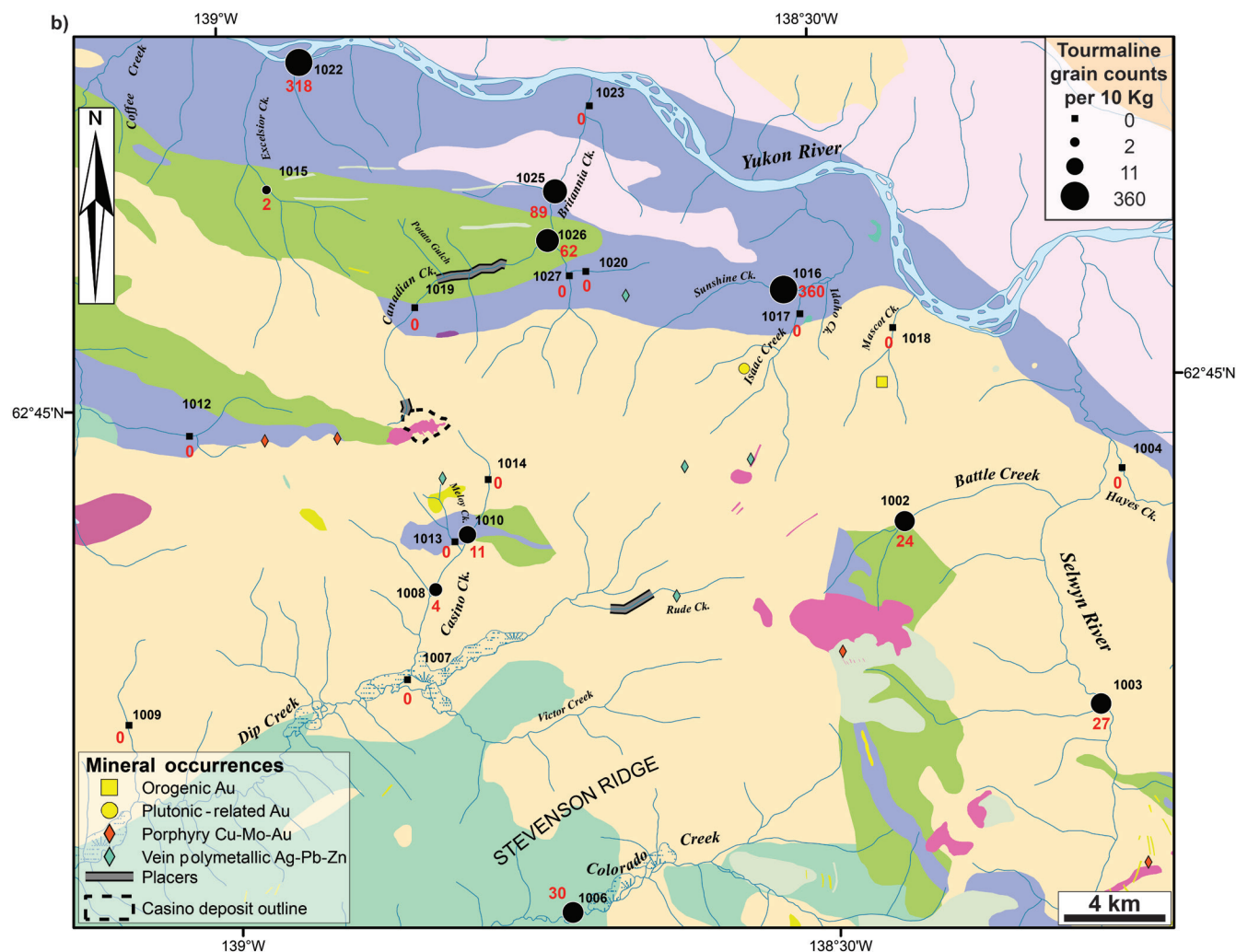


Figure 1. (cont.) b) the location of stream-sediment sample sites (black sample numbers) around the Casino deposit, Yukon, and abundance of tourmaline (grain counts, normalized to 10 kg, in red) in the 2.8 to 3.2 SG, 0.25 to 0.5 mm fraction. See McClenaghan et al. (this volume) for Casino bedrock geology.

Trace-element chemistry

In-situ trace-element analyses of tourmaline were carried out using laser-ablation inductively coupled plasma mass spectrometry (LA-ICP-MS) at Laurentian University. Samples were ablated using a Resonetics RESolution M-50 laser ablation system coupled to a Thermo Fisher XSeries 2 quadrupole ICP-MS. The Resonetics laser uses a 193 nm argon fluoride excimer laser operated at a rate of 8 Hz for line scans with a 30 μm beam and a scan speed between 10 and 15 $\mu\text{m/s}$ with a measured fluence of approximately 3 J/cm². External reference materials included NIST 610 (Jochum et al., 2011), NIST 612 (Jochum et al., 2011), and BHVO2G (Raczek et al., 2001). The NIST 610 standard was used as the primary reference material with Si as the internal standard (values collected from SEM-EDS were used for Si). Drift and data reproducibility were assessed using

NIST 612, BHVO2G, and an in-house tourmaline standard. Standards were ablated before and after each 10 to 15 tourmaline sample analysis. Drift correction was applied using the baseline reduction scheme in iolite (Paton et al., 2011). Samples were analyzed for major and trace elements, including ⁷Li, ⁹Be, ¹¹B, ²⁸Si, ³¹P, ³³S, ³⁹K, ⁴⁵Sc, ⁴⁷Ti, ⁵¹V, ⁵²Cr, ⁵⁵Mn, ⁵⁹Co, ⁶⁰Ni, ⁶⁵Cu, ⁶⁶Zn, ⁷¹Ga, ⁷²Ge, ⁷⁵As, ⁸⁵Rb, ⁸⁸Sr, ⁸⁹Y, ⁹⁰Zr, ⁹³Nb, ⁹⁵Mo, ¹⁰⁷Ag, ¹¹⁵In, ¹¹⁸Sn, ¹²¹Sb, ¹³³Cs, ¹³⁷Ba, ¹³⁹La, ¹⁴⁰Ce, ¹⁴¹Pr, ¹⁴⁶Nd, ¹⁴⁷Sm, ¹⁵³Eu, ¹⁵⁷Gd, ¹⁵⁹Tb, ¹⁶³Dy, ¹⁶⁵Ho, ¹⁶⁶Er, ¹⁶⁹Tm, ¹⁷²Yb, ¹⁷⁵Lu, ¹⁷⁸Hf, ²⁰⁸Pb, ²³²Th, and ²³⁸U. A summary of the trace-element data is presented in Table 2 for bedrock samples and Table 3 for surficial sediment samples. Data on a large number of elements were collected to create a baseline for future comparison.

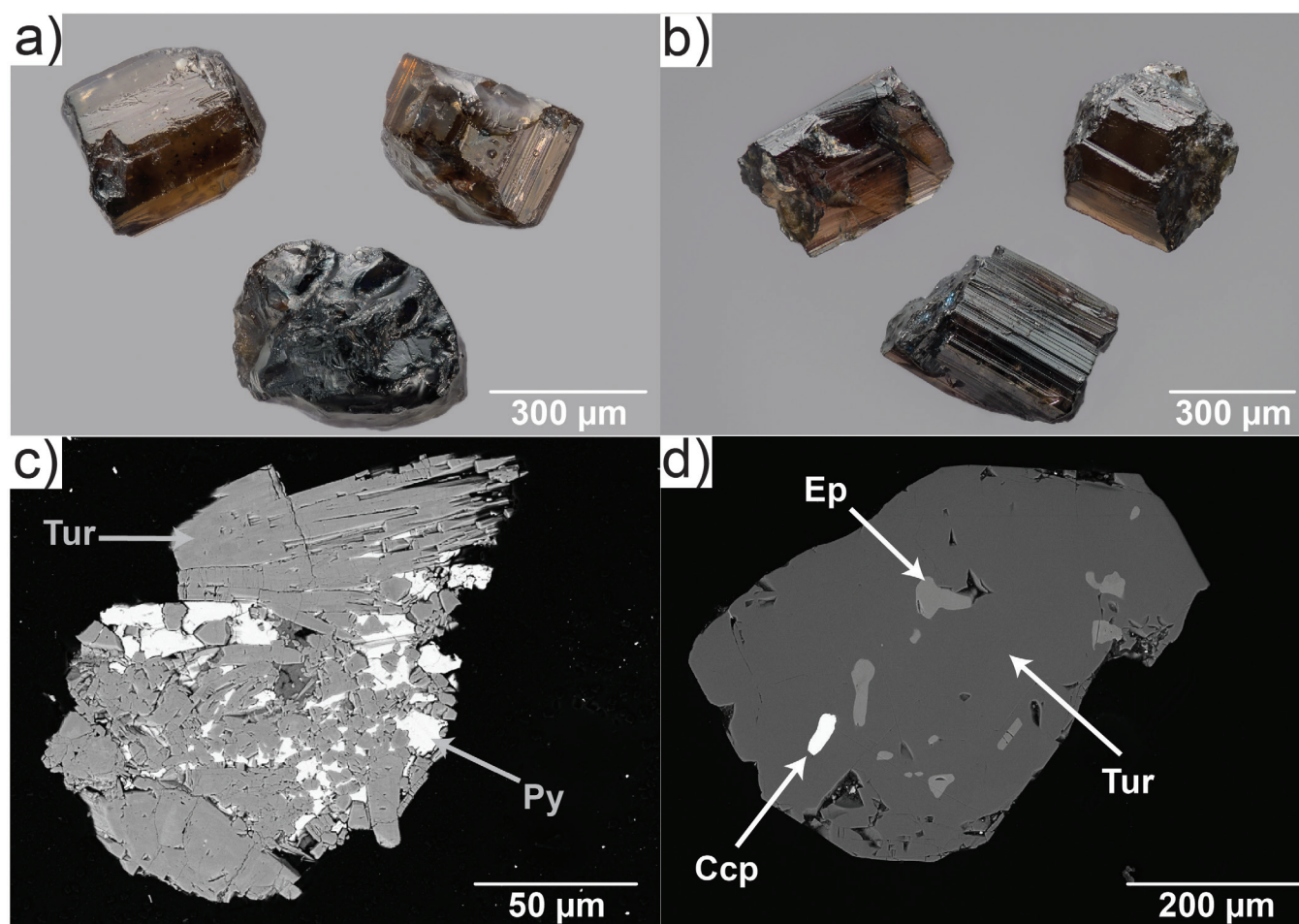


Figure 2. Brown tourmaline grains from the mid-density (2.8–3.2 SG) fraction of: **a)** Geological Survey of Canada (GSC) till sample 11-PMA-009A01, collected less than 1 km northwest (up-ice) of a Woodjam cluster mineralized zone (photograph by Michael J. Bainbridge Photography); **b)** GSC stream-sediment sample 1003, collected downstream of the Cockfield porphyry occurrence, 30 km east of the Casino deposit (photograph by Michael J. Bainbridge Photography); **c)** backscattered electron image of a tourmaline (Tur) grain (from Woodjam till sample 11PMA012A01) infilled by pyrite (Py); and **d)** backscattered electron image of a tourmaline grain (from Casino stream-sediment sample 1025) containing inclusions of chalcopyrite (Ccp) and epidote (Ep).

RESULTS

Tourmaline textures

Bedrock samples

Three distinct styles of bedrock tourmaline have been recognized in samples from Casino and Woodjam: breccia, vein, and disseminated (Fig. 3). One important characteristic is that all three styles of tourmaline can be associated with sulfide mineralization. Sulfides, including chalcopyrite and pyrite, were observed overgrowing prismatic to acicular, subhedral to euhedral tourmaline crystals. Alteration minerals (quartz and albite) are also observed overgrowing euhedral tourmaline crystals; therefore, tourmaline is interpreted to be

one of the earliest forming hydrothermal phases (Fig. 4). In hand sample, tourmaline ranges in colour from usually dark-coloured or black to occasionally colourless and is generally massive in form. Examination of tourmaline in PTS using backscattered-electron (BSE) imaging reveals evidence of complex chemical zonation, dissolution, overgrowths and various mineral inclusions (rutile, ilmenite, quartz, and apatite), although inclusions are generally rare. Although typically black in hand sample, in thin section under cross-polarized light tourmaline can range from brown, pale green to green, blue, or nearly colourless. Pleochroism is generally weak in comparison to that observed in tourmaline from other geological settings; porphyry tourmaline pleochroism is colourless to blue-green in most cases.

Table 1. Representative major element compositions of tourmaline from bedrock, till, and stream-sediment samples collected at the Woodjam and Casino deposits. Values are in *apfu*.

	13CDB-WJ09 C2 6-2	13CDB-WJ05 C2 4-1	CEBB-031 C32-3	CEBB-005 C2 4-1	CEBB-7 SOI1-4 2	11PMA-009-01	12PMA-126A-01	Casino-1010-A6	Casino-1026-B1
Deposit	Woodjam	Woodjam	Casino	Casino	Casino	Woodjam	Woodjam	Casino	Casino
Sample type	Bedrock	Bedrock	Bedrock	Bedrock	Bedrock	Till	Till	Stream sediment	Stream sediment
SiO ₂	35.88	34.27	37.76	38.76	36.33	37.18	36.50	36.30	36.13
TiO ₂	0.33	0.93	0.38		0.22	0.48	0.68	0.80	0.68
Al ₂ O ₃	30.70	20.46	33.03	36.41	34.97	32.65	32.57	34.39	29.61
FeO	9.17	18.96	7.55	2.12	0.45	6.02	5.47	3.98	8.21
MgO	7.03	7.79	6.83	9.55	10.58	7.03	8.11	7.49	8.41
CaO	1.46	3.04				0.15	0.46	0.94	1.74
Na ₂ O	1.78	1.43	2.63	2.24	2.70	2.36	2.40	1.77	2.21
Si(T)	5.949	5.938	6.059	5.952	5.806	6.093	5.947	5.912	5.960
Al(T)	0.051	0.004	0.000	0.048	0.194	0.000	0.053	0.088	0.040
B(T)	0.000	0.058	0.000	0.000	0.000	0.000	0.000	0.000	0.000
Al(Z)	5.949	4.175	0.247	6.000	6.000	6.000	6.000	6.000	5.716
Mg(Z)	0.051	1.825	0.000	0.000	0.000	0.000	0.000	0.000	0.284
Al(Y)	0.000	0.000	0.247	0.541	0.393	0.305	0.202	0.511	0.000
Ti(Y)	0.042	0.122	0.046	0.000	0.026	0.060	0.084	0.098	0.085
Mg(Y)	1.686	0.188	1.634	2.186	2.520	1.717	1.969	1.819	1.783
Fet(Y)	1.272	2.748	1.013	0.273	0.060	0.825	0.745	0.541	1.132
Ca(X)	0.259	0.564	0.000	0.000	0.000	0.027	0.081	0.164	0.307
Na(X)	0.572	0.480	0.818	0.666	0.835	0.749	0.758	0.558	0.707
Vac	0.169	0.000	0.182	0.334	0.165	0.224	0.161	0.279	0.000

Note: *apfu* (atoms per formula unit) calculated based on 31 anions; Vac: vacancy.

Tourmaline breccias

Tourmaline breccias are the most widely recognized style of tourmaline in porphyry deposits (Sillitoe, 2010); this is consistent with our observations in this study. The tourmaline develops as a matrix material, cementing the breccia (Fig. 3a). Although the matrix can be greater than 90% tourmaline, quartz and sulfides (chalcopyrite and pyrite) that postdate the tourmaline may also be present as matrix cement. The tourmaline grains in the breccia typically develop as radial aggregates of prismatic to acicular crystals that average approximately 50 μm but range from sub-micron up to millimetres in diameter in rare cases. We observed grains to be colour zoned in cross section and along their length.

Tourmaline in veins

The crystals in tourmaline in veins (Fig. 3b) are the smallest among the three tourmaline mineralization styles, typically approximately 20 μm in diameter and only rarely up to 100 μm in length. This tourmaline commonly develops in veins (millimetres to centimetres in vein thickness)

associated with paragenetically later quartz and sulfide. The veins are variable in width and commonly have bleached white selvages, mainly of feldspar and quartz (Fig. 3b). Tourmaline grains are randomly oriented with respect to vein margins and tend to occur in densely packed aggregates, the interstices of which are predominantly occupied by quartz and, to a lesser extent, sulfides.

Disseminated tourmaline

Of the three styles observed in the porphyry system, disseminated tourmaline (Fig. 3c) forms the largest crystals, with grains up to several centimetres in length. Texturally, disseminated tourmaline closely resembles tourmaline breccia (i.e. acicular to prismatic radiating masses, commonly infilled by quartz), but the tourmaline develops in discrete anhedral clots instead of the radiating interlocking masses observed in breccias. Some of the clots appear to represent the dissolution of pre-existing phases (feldspar?), based on the shape of the cavities they infill. Disseminated tourmaline can also be found in association with paragenetically later sulfides (pyrite and chalcopyrite).

Table 2. Summary of trace-element analyses in tourmaline from bedrock samples collected from the Casino and Woodjam deposits.

Element	Abundance (ppm)						
	Samples above LOD	Av. LOD (ppm)	Minimum	Maximum	Mean	Median	Standard deviation
³⁹ K	145	20	73	6900	600	240	915
⁴⁵ Sc	145	1	7	250	56	46	40
⁴⁷ Ti	145	5	111	5150	1688	1521	932
⁵¹ V	145	2	85	1175	439	389	217
⁵² Cr	143	0.1	< LOD	347	50.5	39.1	52.4
⁵⁵ Mn	145	3	21	1300	152	79	186
⁵⁹ Co	145	0.1	0.6	260	14.2	5.4	25.6
⁶⁰ Ni	145	0.1	0.2	31.7	12.8	10.9	8.4
⁶⁵ Cu	140	0.1	< LOD	510	37.8	19.0	68.1
⁶⁶ Zn	145	0.1	5.7	151	34.0	20.1	28.1
⁶⁹ Ga	145	0.1	21.5	103	47.7	47.1	12.3
⁷² Ge	145	0.1	0.8	13.9	5.4	5.2	2.5
⁷⁵ As	143	1	< LOD	322	37.7	21.8	48.7
⁸⁵ Rb	134	0.2	< LOD	25.8	2.4	0.8	4.4
⁸⁸ Sr	145	0.2	34.8	623	209.6	164	143.2
⁸⁹ Y	143	0.03	< LOD	73	6.6	2.9	11.5
⁹⁰ Zr	145	0.1	0.6	45.0	5.3	2.2	7.8
⁹³ Nb	143	0.2	< LOD	2.9	0.7	0.6	0.6
⁹⁵ Mo	143	0.1	< LOD	51	4.6	1.3	6.6
¹¹⁵ In	140	0.01	< LOD	1.4	0.3	0.2	0.2
¹¹⁸ Sn	145	0.5	1.3	57.0	17.1	16.5	10.9
¹²¹ Sb	143	0.2	< LOD	41.5	2.4	0.9	5.3
¹³⁷ Ba	143	0.2	< LOD	300	17.4	5.4	35.6
¹³⁹ La	143	0.03	< LOD	15.20	3.02	2.01	3.31
¹⁴⁰ Ce	145	0.03	0.05	29.4	5.14	2.80	5.63
¹⁴¹ Pr	143	0.03	< LOD	3.7	0.47	0.25	0.56
¹⁴⁶ Nd	142	0.01	< LOD	13.80	1.59	0.72	2.00
¹⁴⁷ Sm	104	0.01	< LOD	4.20	0.31	0.17	0.52
¹⁵³ Eu	136	0.03	< LOD	0.34	0.09	0.08	0.06
¹⁵⁷ Gd	114	0.01	< LOD	9.8	0.49	0.18	1.13
¹⁵⁹ Tb	119	0.03	< LOD	1.91	0.10	0.04	0.23
¹⁶³ Dy	132	0.01	< LOD	13.8	0.88	0.35	1.83
¹⁶⁵ Ho	133	0.03	< LOD	2.69	0.24	0.11	0.42
¹⁶⁶ Er	142	0.01	< LOD	7.98	0.90	0.49	1.33
¹⁶⁹ Tm	140	0.03	< LOD	1.30	0.16	0.10	0.20
¹⁷² Yb	143	0.01	< LOD	10.8	1.49	1.04	1.54
¹⁷⁵ Lu	141	0.03	< LOD	1.63	0.28	0.21	0.25
¹⁷⁸ Hf	131	0.04	< LOD	2.53	0.31	0.12	0.48
²⁰⁸ Pb	143	0.04	< LOD	11.50	2.55	1.37	2.70
²³² Th	143	0.04	< LOD	18.00	1.26	0.59	1.82
²³⁸ U	135	0.04	< LOD	1.59	0.37	0.28	0.31

LOD: limit of detection

Table 3. Summary of trace-element analyses in tourmaline grains from surficial sediment samples collected surrounding the Casino and Woodjam deposits.

Element	Samples above LOD	Abundance (ppm)					
		Av. LOD (ppm)	Minimum	Maximum	Mean	Median	Standard deviation
³⁹ K	1373	20	< LOD	2900	315	252	265
⁴⁵ Sc	1565	1	< LOD	993	27	11	56
⁴⁷ Ti	1585	5	108	70000	4645	4540	2791
⁵¹ V	1583	2	< LOD	18900	404	227	921
⁵² Cr	1575	0.1	< LOD	7200	333	243	466
⁵⁵ Mn	1584	3	< LOD	12900	164	76	434
⁵⁹ Co	1572	0.1	< LOD	114	23.5	19.4	16.1
⁶⁰ Ni	1542	0.1	< LOD	672	69.3	45.4	70.4
⁶⁵ Cu	1377	0.1	< LOD	2100	27.1	7.9	107.9
⁶⁶ Zn	1585	0.1	10.3	3020	201	169	178
⁶⁹ Ga	1582	0.1	< LOD	187	37.2	32.4	18.8
⁷² Ge	1200	0.1	< LOD	25	2.5	1.6	2.8
⁷⁵ As	1325	1	< LOD	670	7	3	26
⁸⁵ Rb	1140	0.2	< LOD	31.0	1.5	0.6	3.1
⁸⁸ Sr	1584	0.2	< LOD	2740	300	229	261
⁸⁹ Y	1277	0.03	< LOD	378	1.22	0.11	12.20
⁹⁰ Zr	1516	0.1	< LOD	6200	13.1	0.6	196
⁹³ Nb	1415	0.2	< LOD	340	0.8	0.1	9.2
⁹⁵ Mo	1369	0.1	< LOD	150	21.4	0.6	4.4
¹¹⁵ In	1108	0.01	< LOD	4.80	0.14	0.04	0.36
¹¹⁸ Sn	1544	0.5	< LOD	497	6.6	1.7	23.1
¹²¹ Sb	1362	0.2	< LOD	360	1.1	0.3	9.9
¹³⁷ Ba	1309	0.2	< LOD	460	6.1	0.9	23.2
¹³⁹ La	1543	0.03	< LOD	21.80	1.90	1.00	2.60
¹⁴⁰ Ce	1555	0.03	< LOD	77.00	3.23	1.60	4.90
¹⁴¹ Pr	1381	0.03	< LOD	4.30	0.33	0.17	0.47
¹⁴⁶ Nd	1283	0.01	< LOD	11.60	1.15	0.59	1.61
¹⁴⁷ Sm	541	0.01	< LOD	4.40	0.27	0.13	0.42
¹⁵³ Eu	1362	0.03	< LOD	2.48	0.39	0.30	0.36
¹⁵⁷ Gd	427	0.01	< LOD	5.50	0.24	0.10	0.48
¹⁵⁹ Tb	345	0.03	< LOD	1.50	0.04	0.04	0.48
¹⁶³ Dy	332	0.01	< LOD	18.00	0.39	0.06	1.49
¹⁶⁵ Ho	291	0.03	< LOD	11.60	0.15	0.04	0.78
¹⁶⁶ Er	266	0.01	< LOD	70.00	0.86	0.06	1.74
¹⁶⁹ Tm	211	0.03	< LOD	16.20	0.25	0.04	1.24
¹⁷² Yb	268	0.01	< LOD	158	1.89	0.10	10.91
¹⁷⁵ Lu	274	0.03	< LOD	31.70	0.41	0.04	2.30
¹⁷⁸ Hf	320	0.04	< LOD	140	1.51	0.15	10.25
²⁰⁸ Pb	1585	0.04	0.27	260	18.73	15.50	15.12
²³² Th	625	0.04	< LOD	12.70	0.41	0.06	1.02
²³⁸ U	596	0.04	< LOD	13.00	0.21	0.05	0.78
LOD: limit of detection							

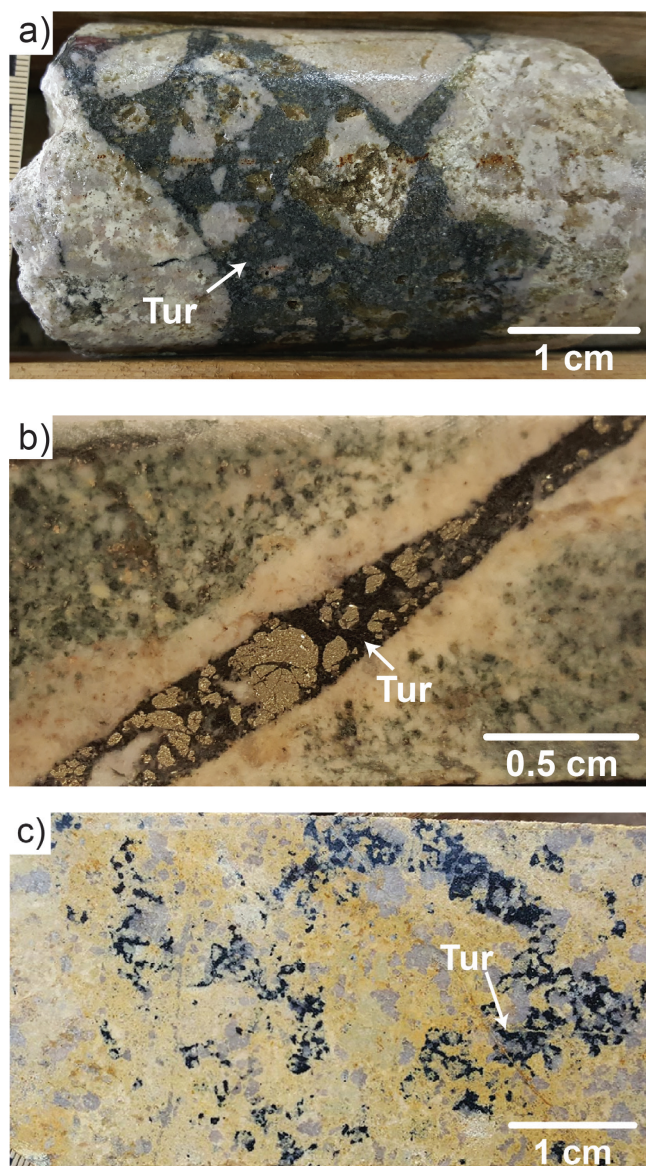


Figure 3. Hand samples of core showing the variable textural styles of tourmaline (Tur) in bedrock: **a)** tourmaline cemented breccia from the Casino deposit (Photograph by C.E. Beckett Brown; NRCAN photo 2020-128); **b)** tourmaline from the Woodjam deposit cluster forming as monomineralic veins (Photograph by C.E. Beckett-Brown; NRCAN photo 2020-129); **c)** tourmaline from the Casino deposit forming as isolated disseminated clots (Photograph by C.E. Beckett-Brown; NRCAN photo 2020-130).

Surficial sediment samples

Tourmaline recovered from surficial sediment samples is predominantly subhedral and brown to black in colour, or rarely yellow, green, or blue (Fig. 2a, b). In general, tourmaline occurs in sediments as individual grains and only rarely as agglomerations (Fig. 2c). The types of mineral inclusions identified in detrital tourmaline grains are summarized in Table 4 for the Woodjam deposit and Table 5 for the Casino deposit. Of the 1545 tourmaline grains examined, 60%

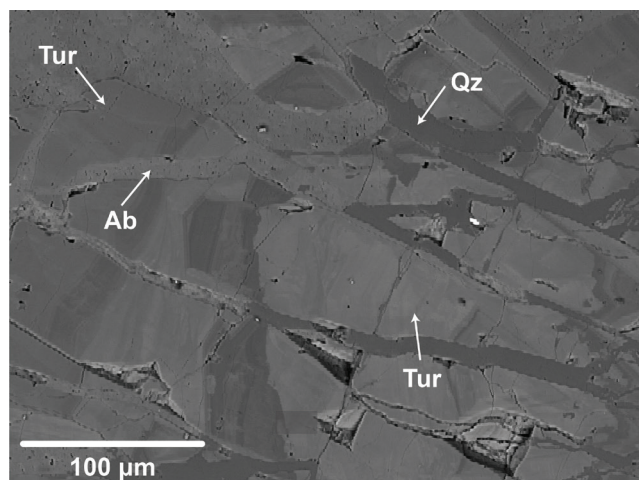


Figure 4. Backscattered-electron image showing the paragenetic position of tourmaline. Tur: tourmaline; Ab: albite; Qz: quartz.

contained mineral inclusions; most are (listed in decreasing abundance) zircon, quartz, rutile, ilmenite, epidote, and chalcopyrite (e.g. Fig. 2d). There are differences in the type and abundance of inclusions at the two study areas. At Woodjam, approximately 50% of the grains contain inclusions (Table 4) and at Casino, approximately 75% of detrital grains contain inclusions (Table 5). Ilmenite inclusions are twice as common in Woodjam tourmaline grains than in Casino tourmaline grains, but pyrite is more abundant in the Casino tourmaline. Detrital tourmaline grains also contain inclusions or attached grains of pyrite (Fig. 2c), chalcopyrite, galena, sphalerite, jarosite, or barite.

Mineral chemistry

Backscattered electron imaging

Tourmaline in bedrock

Minerals in the tourmaline supergroup are able to accommodate a wide range of elements during their crystallization histories (van Hinsberg et al., 2011). The tourmaline from Casino and Woodjam bedrock samples examined in this study exhibits, in general, a high degree of chemical heterogeneity and zonation. These grain-scale features are best observed with BSE imaging, which highlights differences in average atomic number in a given sample. Based on BSE imaging, four types of compositional growth textures are observed in the bedrock samples (Fig. 5). These textures are further subdivided by whether they are likely to be primary (developed at the time of crystallization) or secondary (developed post-crystallization) in origin, as suggested by Slack and Trumbull (2011). Primary features are oscillatory/concentric growth zoning, interpreted to reflect changes in local fluid composition, displaying sharp chemical boundaries or zones developed parallel to [001] (Fig. 5a); and sector/polar zoning that reflects selective partitioning of elements in distinct

Table 4. Mineral inclusions identified in detrital tourmaline grains collected from till at the Woodjam deposit.

Sample number		Total grains	Grains with inclusions	Zircon	Quartz	Rutile	Ilmenite	Biotite	Apatite	Alanite	Epidote	Muscovite	Fe-oxide	Albite	Chlorite	Apatite-REE	Pyrite	K-feldspar	Dumortierite	Titanite	Pentlandite	Ferrosilite	Galena	Calcite	Barite		
All samples	# grains	1122	597	251	231	96	65	40	39	38	30	25	17	14	14	14	14	13	6	6	3	1	1	1	1		
	%	–	53.2	22.4	20.6	8.6	5.8	3.6	3.5	3.4	2.7	2.2	1.5	1.3	1.3	1.3	1.2	0.5	0.5	0.3	<0.1	<0.1	<0.1	<0.1			
11PMA003A03	# grains	40	22	9	9	4	1	1	1	–	–	–	–	–	–	1	–	1	–	–	–	–	–	–	–		
	%	–	55	22.5	22.5	10.0	2.5	2.5	2.5	–	–	–	–	–	–	2.5	–	2.5	–	–	–	–	–	–	–		
11PMA007A01	# grains	70	34	13	11	4	3	2	1	4	1	–	–	1	1	1	–	2	–	–	–	–	–	–	–		
	%	–	48.6	18.6	15.7	5.7	4.3	2.9	1.4	5.7	1.4	–	–	1.4	1.4	1.4	–	2.9	–	–	–	–	–	–	–		
11PMA009A01	# grains	71	40	14	15	8	3	2	3	1	3	–	1	1	2	–	–	–	–	–	1	1	–	–	–		
	%	–	56.3	19.7	21.1	11.3	4.2	2.8	4.2	1.4	4.2	–	1.4	1.4	2.8	–	–	–	–	–	1.4	1.4	–	–	–		
11PMA012A01	# grains	28	13	3	4	2	1	–	1	1	1	–	5	1	–	–	–	–	–	–	–	–	–	–	–		
	%	–	46.4	10.7	14.3	7.1	3.6	–	3.6	3.6	3.6	–	17.9	3.6	–	–	–	–	–	–	–	–	–	–	–		
12PMA117A01	# grains	67	42	21	12	9	5	3	3	1	–	–	–	–	–	1	1	1	1	1	–	–	–	–	–		
	%	–	62.7	31.3	17.9	13.4	7.5	4.5	4.5	1.5	–	–	–	–	–	1.5	1.5	1.5	1.5	–	–	–	–	–	–		
12PMA126A01	# grains	93	40	15	17	7	3	3	3	3	2	5	1	–	1	–	–	–	2	–	–	–	1	–	–		
	%	–	43	16.1	18.3	7.5	3.2	3.2	3.2	3.2	2.2	5.4	1.1	–	1.1	–	–	–	2.2	–	–	1.1	–	–	–		
12PMA593A01	# grains	67	37	12	16	5	3	1	1	3	1	1	–	–	1	3	1	–	1	–	–	–	–	–	–		
	%	–	55.2	17.9	23.9	7.5	4.5	1.5	1.5	4.5	1.5	1.5	–	–	1.5	4.5	1.5	–	1.5	–	–	–	–	–	–		
12PMA128A01	# grains	92	53	26	19	8	4	3	2	–	5	2	5	2	3	1	2	–	1	–	–	–	–	–	–		
	%	–	57.6	28.3	20.7	8.7	4.3	3.2	2.2	–	5.4	2.2	5.4	2.2	3.2	1.1	2.2	–	1.1	–	–	–	–	–	–		
12PMA594A01	# grains	99	44	14	19	6	5	3	3	–	5	1	1	2	–	–	1	–	–	–	–	–	–	–	–		
	%	–	44.4	14.1	19.2	6.1	5.1	3.0	3.0	–	5.1	1.0	1.0	2.0	–	–	1.0	–	–	–	–	–	–	–	–		
12PMA599A01	# grains	95	47	18	21	6	7	4	4	7	1	6	–	1	–	3	3	–	–	–	1	–	1	–	–		
	%	–	49.5	18.9	22.1	6.3	7.4	4.2	4.2	7.4	1.1	6.3	–	1.1	–	3.2	3.2	–	–	1.1	–	–	1.1	–	–		
12PMA603A01	# grains	99	50	23	19	8	4	1	1	3	2	1	–	1	1	–	1	–	–	–	–	–	–	–	–		
	%	–	50.5	23.2	19.2	8.1	4.0	1.0	1.0	3.0	2.0	1.0	–	1.0	1.0	–	1.0	–	–	–	–	–	–	–	–		
12PMA614A01	# grains	42	22	9	8	4	3	1	3	–	–	–	–	–	–	2	2	–	–	–	–	–	–	–	–		
	%	–	52.4	21.4	19.0	9.5	7.1	2.4	7.1	–	–	–	–	–	–	4.8	4.8	–	–	–	–	–	–	–	–		
12PMA615A01	# grains	48	25	10	11	3	1	2	–	1	–	2	2	2	–	–	2	1	–	–	–	–	–	–	–		
	%	–	52.1	20.8	22.9	6.3	2.1	4.2	–	2.1	–	4.2	4.2	4.2	–	–	4.2	2.1	–	–	–	–	–	–	–		
12PMA620A01	# grains	40	27	13	12	8	4	3	1	3	–	1	–	–	–	–	–	–	–	1	–	–	–	–	–		
	%	–	67.5	32.5	30.0	20.0	10.0	7.5	2.5	7.5	–	2.5	–	–	–	–	–	–	–	2.5	–	–	–	–	–		
12TFE114A01	# grains	85	52	26	18	8	6	5	5	6	4	5	1	2	1	1	–	–	1	–	–	–	–	1	–		
	%	–	61.2	30.6	21.2	9.4	7.1	5.9	5.9	7.1	4.7	5.9	1.2	2.4	1.2	1.2	–	–	1.2	–	–	–	–	1.2	–		
12TFE130A01	# grains	86	50	25	20	6	12	6	6	5	5	1	1	1	2	1	2	1	–	–	–	–	–	–	1		
	%	–	58.1	29.1	23.3	7.0	14.0	7.0	7.0	5.8	5.8	1.2	1.2	1.2	2.3	1.2	2.3	1.2	–	–	–	–	–	–	1.2		
				Abbreviations: REE: rare-earth elements																							

Abbreviations: REE: rare-earth elements

Table 5. Mineral inclusions identified in detrital tourmaline grains collected from stream sediments at the Casino deposit.

Sample number	# grains	423	331	Zircon	Rutile	Quartz	Epidote	Fe-oxide	Apatite	Biotite	Muscovite	Pyrite	Apatite-REE	Alanite	Ilmenite	K-feldspar	Barite	Titanite	Albite	Chlorite	Calcopyrite	Jarosite	Galena	Sphalerite	Dumortierite	Zn-staurolite	Molybdenite	Calcite	Dioside
All samples	%	–	78.3	30.5	26.5	17.5	11.3	8.7	8.0	7.8	7.8	7.8	6.4	6.1	5.2	4.0	3.5	2.8	1.9	1.4	1.2	0.9	0.7	0.7	0.7	0.5	0.2	0.2	1
1002	# grains	16	10	1	2	2	–	1	2	–	–	–	–	1	1	2	–	–	–	–	–	–	–	–	–	–	–	–	–
	%	–	62.5	6.3	12.5	12.5	–	6.3	12.5	–	–	–	–	6.3	6.3	12.5	–	–	–	–	–	–	–	–	–	–	–	–	–
1003	# grains	19	12	2	1	3	–	–	2	1	–	–	1	–	1	2	–	1	–	–	–	–	–	–	–	–	–	–	–
	%	–	63.2	11.1	5.6	16.7	–	–	11.1	5.6	–	–	5.6	–	5.6	11.1	–	5.6	–	–	–	–	–	–	–	–	–	–	–
1006	# grains	18	16	4	3	8	2	3	–	–	–	1	1	7	2	3	–	1	–	–	–	–	–	–	1	–	–	–	–
	%	–	88.9	22.2	16.7	44.4	11.1	16.7	–	–	–	5.6	5.6	–	11.1	16.7	–	5.6	–	–	–	–	–	–	5.6	–	–	–	–
1008	# grains	4	4	1	2	3	1	1	–	1	–	–	1	1	–	–	1	–	–	–	–	–	–	–	–	–	–	–	–
	%	–	100.0	25.0	50.0	75.0	25.0	25.0	–	25.0	–	–	25.0	25.0	–	–	25.0	–	–	–	–	–	–	–	–	–	–	–	–
1010	# grains	11	10	5	6	3	1	2	3	3	–	–	–	2	3	–	–	–	–	–	–	–	–	–	–	–	–	–	–
	%	–	90.9	45.5	54.5	27.3	9.1	18.2	27.3	27.3	–	–	–	18.2	27.3	–	–	–	–	–	–	–	–	–	–	–	–	–	–
1015	# grains	3	3	–	1	2	2	–	1	–	–	–	–	3	–	–	–	–	–	–	–	–	–	–	–	–	–	–	–
	%	–	100.0	–	33.3	66.6	–	–	33.3	–	–	–	–	100.0	–	–	–	–	–	–	–	–	–	–	–	–	–	–	–
1016	# grains	92	78	40	28	13	4	8	9	10	10	8	8	5	6	5	4	1	2	1	1	1	1	2	–	–	–	1	–
	%	–	84.8	43.5	30.4	14.1	4.3	8.7	9.8	10.9	10.9	8.7	8.7	5.4	6.5	5.4	4.3	1.1	2.2	1.1	1.1	1.1	1.1	2.2	–	–	–	1.1	–
1022	# grains	150	121	63	46	24	18	10	12	11	16	19	14	5	8	3	5	8	5	3	–	–	–	–	2	2	1	–	1
	%	–	80.7	42.0	30.7	16.0	12.0	6.7	8.0	7.3	10.7	12.7	9.3	3.3	5.3	2.0	3.3	5.3	3.3	2.0	–	0.7	–	–	1.3	1.3	0.7	–	0.7
1025	# grains	52	40	7	14	8	6	7	3	5	3	2	1	–	1	2	3	–	–	1	3	–	–	–	–	–	–	–	–
	%	–	76.9	13.5	26.9	15.4	11.5	13.5	5.7	9.6	5.7	3.8	1.9	–	1.9	3.8	5.7	–	–	1.9	5.7	–	–	–	–	–	–	–	–
1026	# grains	58	37	6	9	8	14	5	2	2	4	3	1	2	–	–	2	1	1	1	1	1	2	1	–	–	–	–	–
	%	–	71.2	10.3	15.5	13.8	24.1	8.6	3.4	3.4	6.9	5.2	1.7	3.4	–	–	3.4	1.7	1.7	1.7	1.7	3.4	1.7	1.7	–	–	–	–	–

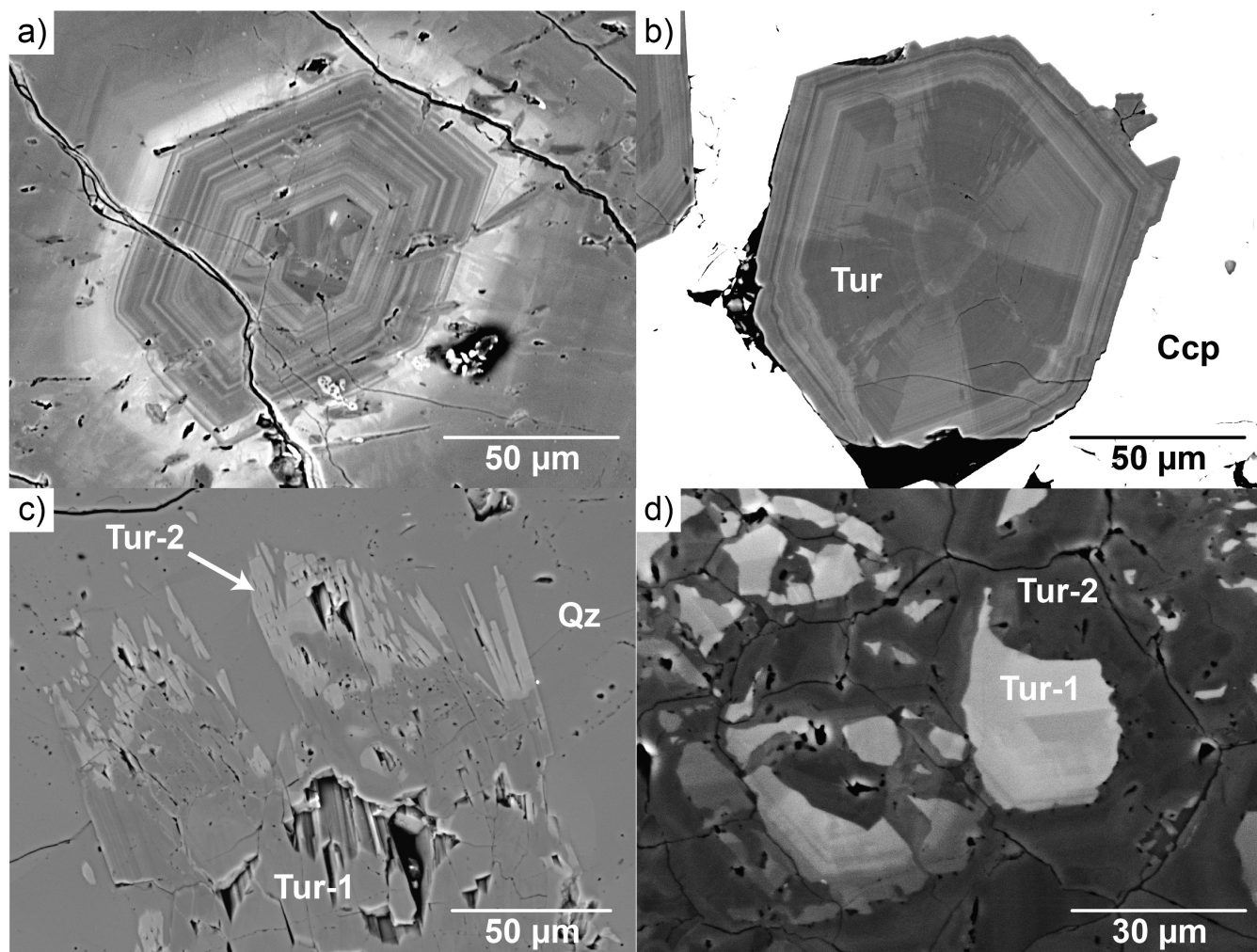


Figure 5. Backscattered-electron images showing the internal textures of tourmaline grains from bedrock samples: **a)** oscillatory zonation; **b)** sector zonation; **c)** overgrowth (Tur-1 is dark, Tur-2 is lighter); **d)** irregular/patchy zonation resulting from recrystallization of pre-existing Tur-1, of which some primary fragments still remain, to Tur-2. The primary chemical difference between Tur-1 and Tur-2 is that Tur-2 contains more Mg than Fe.

sectors (Fig. 5b). Secondary textures are patchy/irregular growth features (Fig. 5c), commonly observed in recrystallized tourmaline, with diffuse grain boundaries, developed perpendicular to [001], and overgrowth or replacement features (Fig. 5d). Coupled dissolution-reprecipitation textures (similar to those developed in minerals such as plagioclase) are not currently included in the classification but could be grouped with the patchy/irregular growth features that result from recrystallization. These dissolution-reprecipitation textures correlate with the change from primary Fe-rich (schorl) compositions to more Mg-rich (dravite) ones. Diffusion-like textures are also occasionally observed (Fig. 6a, b).

Tourmaline in surficial sediments

Tourmaline from surficial samples exhibits a high degree of chemical heterogeneity and zonation at the individual grain scale. All four types of compositional growth textures observed

in bedrock are also observed in grains from the surficial samples, with more than 50% of surficial grains exhibiting some type of chemical zonation. Diffusion-like textures similar to those observed in some of the bedrock tourmaline grains from Woodjam were also observed in surficial grains from samples surrounding the deposit cluster (Fig. 6c).

Major- and minor-element chemistry (SEM-EDS)

Tourmaline in bedrock

Tourmaline from the Casino and Woodjam bedrock samples primarily plot within the compositional space of schorl, dravite, and povondraite, regardless of the deposit or tourmaline textural style. The dominant substitution can be summarized by: $R^2 + Na^+ \leftrightarrow Al^{3+} + \square$ ($R^2 = 0.90$) and $Fe^{2+} + (OH)^- \leftrightarrow Al^{3+} + O^{2-}$ ($R^2 = 0.90$). The average (range)

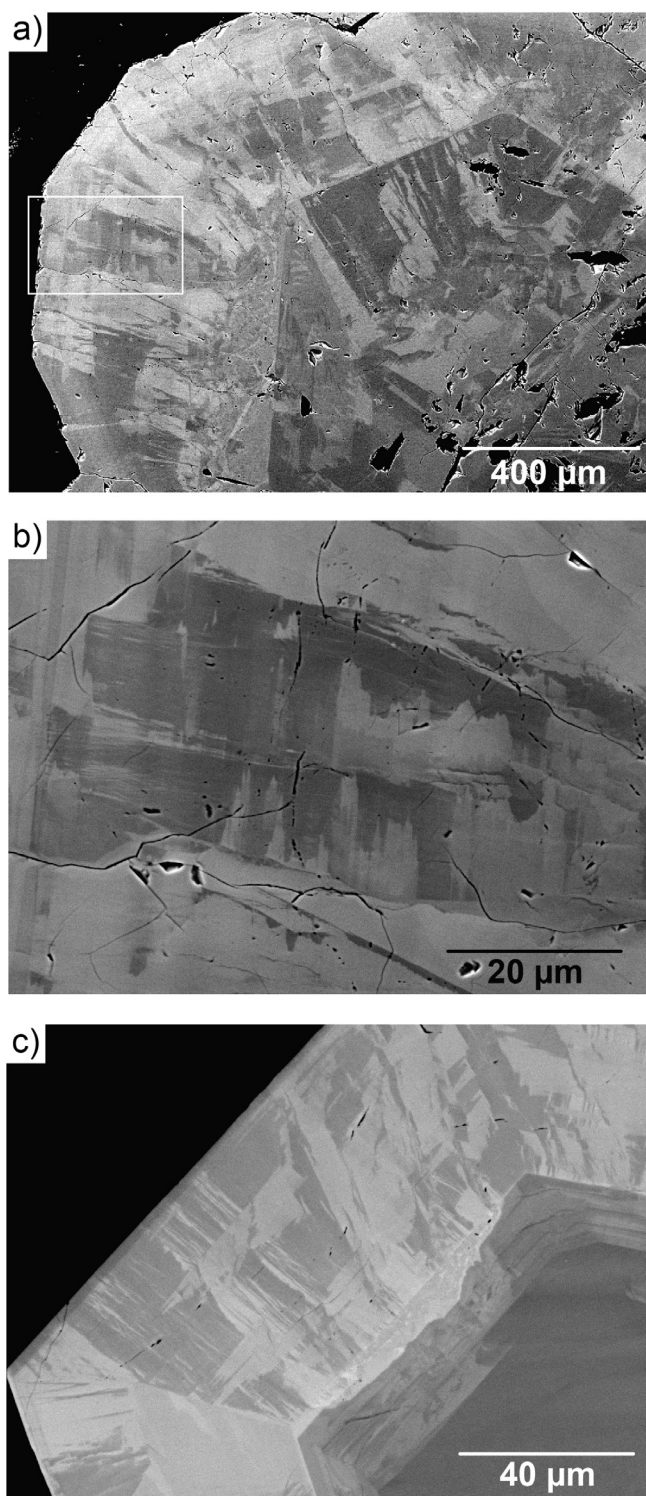


Figure 6. Backscattered-electron images of bedrock and till samples collected at the Woodjam deposit showing tourmaline internal textures in: **a)** a tourmaline grain in a Woodjam bedrock sample showing a combination of oscillatory and sector zoning features as well as some patchy zonation; **b)** magnified view of the white box in **a)** showing patchy zonation; **c)** a tourmaline grain from a till sample near the Woodjam deposit cluster showing similar zonation textures to those observed in the Woodjam bedrock sample in **a)**.

proportions of major elements, expressed in weight per cent, are Na = 1.75 (0.64–2.36), Ca = 0.49 (< LOD–2.64), Ti = 0.27 (< LOD–1.95), Mg = 4.85 (1.60–6.65), Fe = 4.27 (0.20–16.44), Al = 17.19 (10.78–19.90), and Si = 17.20 (15.52–18.68). The average (range) proportions expressed in *apfu* are Na = 0.75 (0.28–1.00), Ca = 0.10 (< LOD–0.70), Ti = 0.03 (< LOD–0.40), Mg = 1.95 (0.69–2.65), Fe = 0.76 (0.04–3.07), Al = 6.24 (4.18–7.14), and Si = 6.01 (5.60–6.55). In general, broad chemical variations conform to the oxy-dravite–povondraite trend, superimposed on a weaker schorl–dravite trend; the oxy-dravite–povondraite trend within this series reflects the increase in Fe³⁺ (and decrease in Al³⁺) that may reflect conditions of increasing oxidation (i.e. *f*O₂; Fig. 7a, b). The predominance of the oxy-dravite–povondraite trend has been previously reported for tourmaline from mineralized porphyry systems in Russia (Baksheev et al., 2012).

Tourmaline in surficial sediments

The chemistry and range in composition determined for detrital tourmaline is similar to that of the tourmaline in bedrock. In terms of end members, most tourmaline grains plot as schorl, dravite, and povondraite, with some grains plotting as uviteferuvite. The average (range) of major elements, expressed in weight per cent, are Na = 1.58 (0.74–2.58), Ca = 0.72 (< LOD–3.17), Ti = 0.43 (< LOD–2.20), Mg = 4.55 (0.13–7.66), Fe = 4.91 (0.21–15.31), Al = 17.43 (12.06–22.92), and Si = 17.19 (15.54–18.88). The average (range) proportions expressed in *apfu* are Na = 0.69 (0.30–1.00), Ca = 0.17 (< LOD–0.75), Ti = 0.08 (< LOD–0.47), Mg = 1.82 (0.05–3.00), Fe = 0.85 (0.04–2.71), Al = 6.27 (4.49–7.71), and Si = 5.95 (5.51–6.21). This shows that there is no clear difference in major- or minor-element chemistry between tourmaline in bedrock and tourmaline in surficial sediments.

Trace-element chemistry

Tourmaline in bedrock

Trace-element analyses (LA-ICP-MS) for 51 elements were completed on 145 tourmaline grains from 15 samples (Table 2). Concentrations of many elements, including Li, Be, Rb, Nb, Mo, Ag, In, Sb, Cs, Ba, Hf, and rare-earth elements (REE), are at or below the lower detection limit. Many, including Co, Ni, Ge, Y, Zr, Sn, Pb, Th, and U, are present in very low concentrations (1–20 ppm), and the remainder, including K, Sc, Ti, V, Cr, Mn, Cu, Zn, Ga, As, and Sr, occur at higher concentrations (hundreds to thousands of parts per million). Significant effort was made to identify relationships between the elements, but very few strong correlations were found. Noteworthy ones include positive correlations between Mn and Zn ($R^2 = 0.61$) and Mn and Sr ($R^2 = 0.48$). It was also found that the trace-element concentration variations in a single, zoned tourmaline grain can be profound,

a)

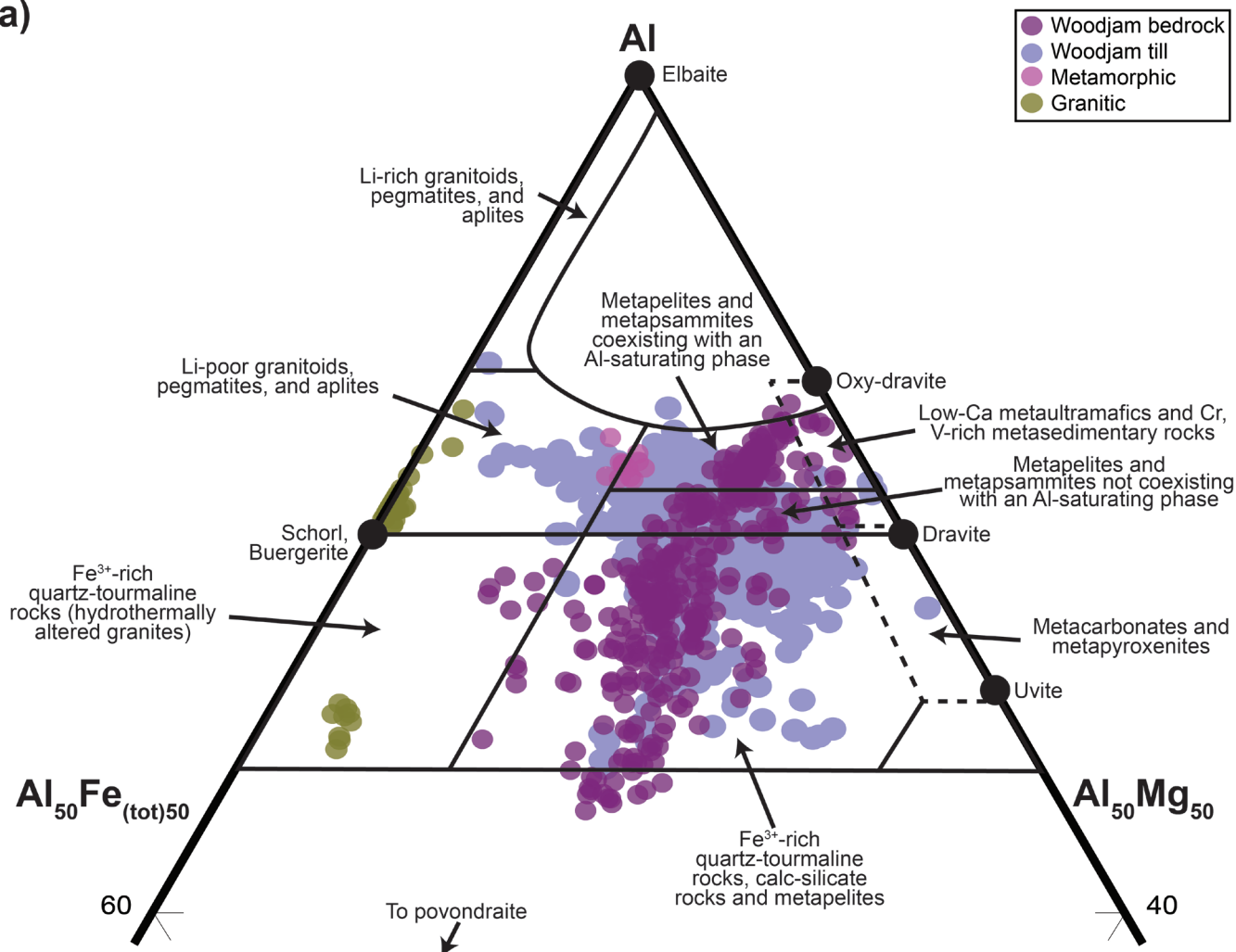


Figure 7. Tourmaline major-element chemistry Al-Mg-Fe for grains from **a)** Woodjam deposit and **b)** Casino deposit bedrock and surficial sediment samples analyzed in this study, plotted using the ternary diagram of Henry and Guidotti (1985). Background unmineralized bedrock is represented by grains classified as metamorphic, from a gneiss from Vador Falls, Ontario, and grains classified as granitic, from the Seagull batholith, Yukon.

with variations of several magnitudes possible. For example, concentrations of Ti, V, and Mn can vary over an order of magnitude, from hundreds to thousands of parts per million, between zones within a grain.

Given the high degree of variation in trace-element concentration from point to point, attempts were made to discern general trends in tourmaline grains through the use of LA-ICP-MS maps, an example of which is shown in Figure 8. The tourmaline grain shown is from the Woodjam deposit and exhibits oscillatory zonation (zones with sharp boundaries developed parallel to [001]) and complex patchy zonation (areas with diffuse boundaries, developed perpendicular to [001]) that in some places crosses oscillatory zone boundaries. Examination of the maps produced for Sc and Mn indicates that elemental distribution is, in part, linked to

oscillatory zonation (Fig. 8). In contrast, high concentrations of other elements, such as Ti, Sr, and Zr, appear to positively correlate with the complex patchy zonation. Closer inspection of Ti and Sr show differences in their zonation patterns, including high concentrations of Ti in the core and intermediate regions but is absent in the rim. Strontium concentrations, in contrast, accentuate the complex zonation throughout the grain and in the rim. In summary, patterns in trace elements are very complex and may or may not correlate with the observed zonation type in all cases.

Tourmaline in surficial sediments

A total of 1585 tourmaline grains were analysed from 26 surficial sediment samples from Casino and Woodjam (Table 3). Some of the elements analyzed occur at or below

b)

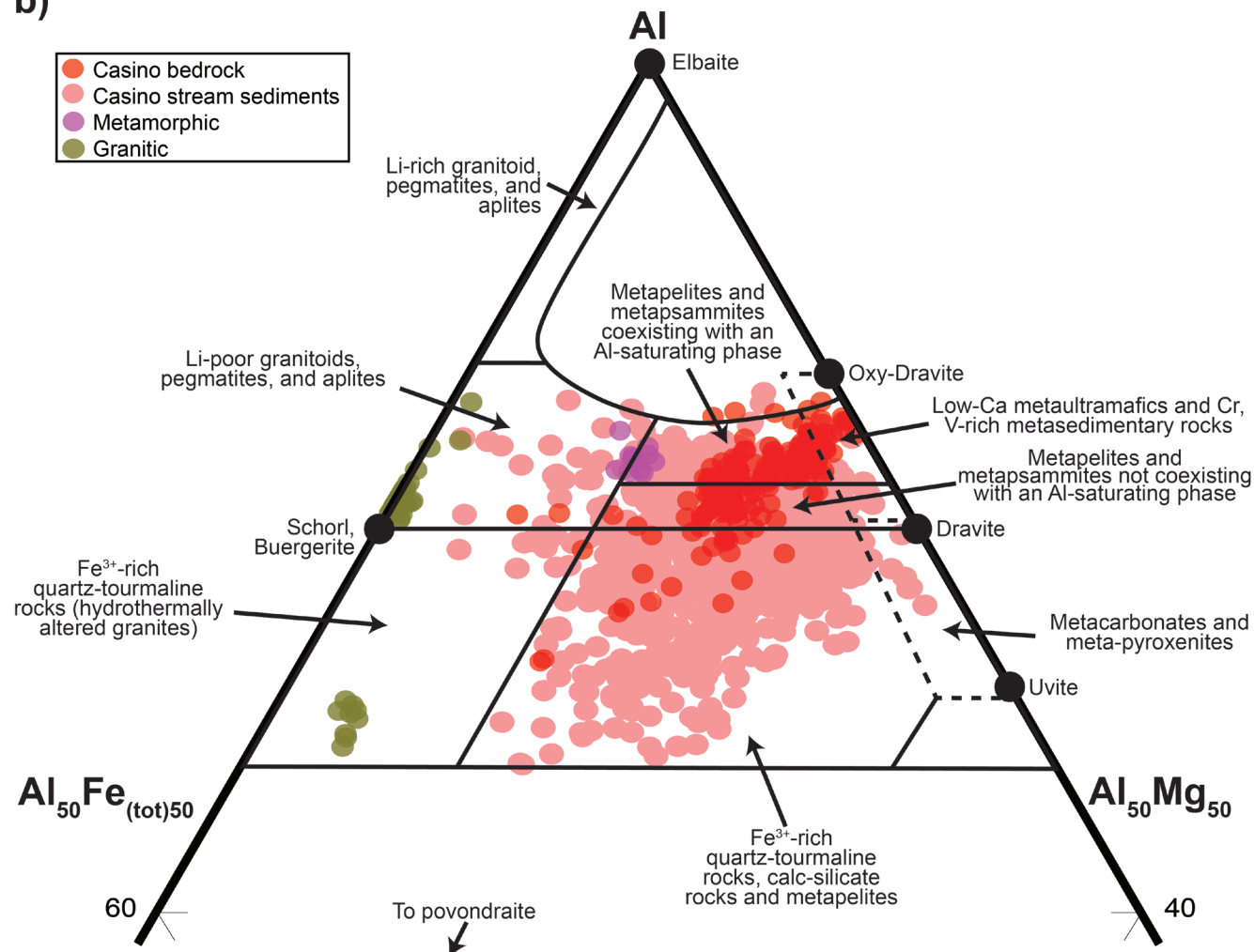


Figure 7. (cont.)

the lower detection limit, including Li, Be, Rb, Nb, Mo, Ag, In, Sb, Cs, Ba, Hf, and REE. The average concentration range of Co, Cu, Ge, As, Y, Zr, Sn, Pb, Th, and U is 1 to 20 ppm, whereas K, Sc, Ti, V, Cr, Mn, Ni, Zn, Ga, and Sr occur in much higher concentrations (hundreds to thousands of parts per million). The positive correlations between Mn and Zn and Mn and Sr observed in tourmaline from bedrock samples were not found in tourmaline grains from surficial sediments; however, a correlation between Co and Ni ($R^2 = 0.74$), not noted in the bedrock material, was observed.

DISCUSSION

Using tourmaline as an indicator for mineralized porphyry systems necessarily involves identification of key features in the mineralized bedrock samples, examination of grains from the surficial sediments to search for these same features, and comparison of these features in tourmaline from a variety of geological settings (i.e. pegmatites; granites; and

VMS, orogenic Au, and Sn-W deposits). Observations made as part of this study and a compilation of material from the published literature is provided.

Tourmaline is commonly black in most rock types, except in pegmatites, in which it can be green, blue, pink, and yellow. The tourmaline from mineralized porphyry systems in this study was predominantly black and, less often, was pale brown or colourless. The grain size of tourmaline in bedrock from all geological environments is highly variable and is not a distinctive feature, but the largest tourmaline grains form in pegmatite and granitic settings. Fibrous tourmaline is a morphology not observed in porphyry deposits; it is most typically associated with felsic pegmatites (Dutrow and Henry, 2017). The colour of tourmaline grains under plain polarized light (PPL) can range from browns to greens, blues, and yellows to colourless. A comprehensive analysis of inclusions found within tourmaline does not exist. Zircon appears to be a ubiquitous inclusion in tourmaline from all geological settings, as is quartz. The morphology of quartz

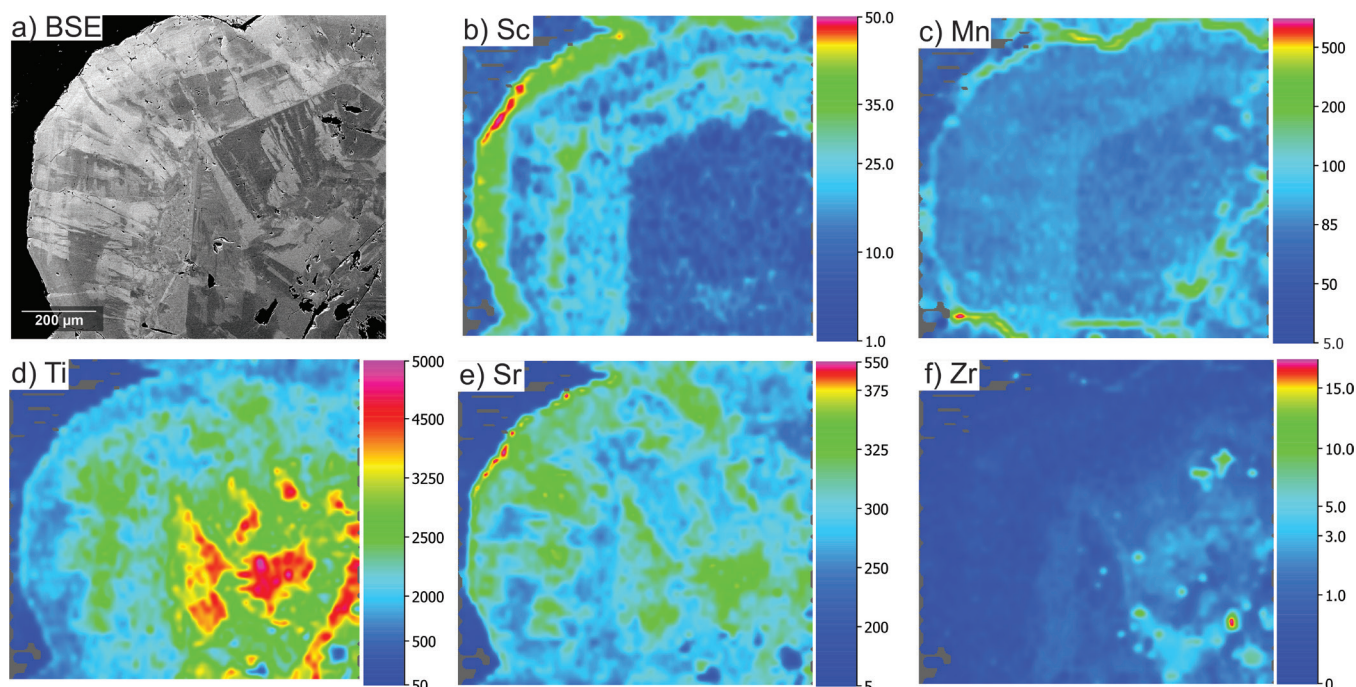


Figure 8: Single Woodjam bedrock-sourced tourmaline grain: **a)** backscatter electron image; **b) to f)** laser-ablation inductively coupled plasma mass spectrometry maps of trace-element content showing **b) Sc**, **c) Mn**, **d) Ti**, **e) Sr**, and **f) Zr**. Element scales are semi-quantitative (parts per million) and indicate relative changes in element concentrations.

inclusions is variable; however, anhedral, well rounded quartz grains often occur in tourmaline derived from metamorphic terranes, and subhedral to euhedral quartz grains are found in tourmaline from most other geological environments. Tourmaline from porphyry deposits does not contain rounded inclusions of quartz.

Tourmaline grains can also be classified using internal growth textures. The presence of complex growth features, such as those observed in the tourmaline crystals analyzed in this study, can be useful for graphically documenting the variations in pressure-temperature-time (P-T-X) experienced by an evolving crystal (Slack and Trumbull, 2011). Oscillatory and sector zonation is widely observed in tourmaline from a range of geological settings, but the presence of patchy/irregular to even ‘chaotic’ growth features is not common, based on our observations during this study and analyses of the existing literature, and appears to be unique to mineralized systems. All tourmaline grains from mineralized porphyry systems examined in this study exhibited zonation of one type or another, including both oscillatory and sector zonation; patchy or irregular zonation within oscillatory or sector zones was also observed (Fig. 6, 8a). The patchy zonation is particularly unusual; it does not destroy the primary oscillatory or sector zonation, which suggests it is unlikely to be a product of recrystallization. It is possible that patchy zonation (Fig. 6) is produced through chemical diffusion; however, this idea appears to be at odds with the commonly accepted view that diffusion is negligible (Palmer et al., 1992; Henry and Dutrow, 1996). Still, degrees

of chemical diffusion involving major and some trace elements have been noted in tourmaline that has undergone deformation under moderate to high-grade conditions (e.g. mylonite metamorphosed to the amphibolite facies; Büttner and Kasemann, 2007). Tourmaline has also exhibited greater diffusion along the c-axis (Desbois and Ingrin, 2007). For bedrock samples in this study, the effect of deformation can be ignored because the rocks are undeformed. Diffusion features, if present, align well with the orientation perpendicular to [001] of the grains from this study (Fig. 6, 8). The orientation of these diffusion features could also be related to the weak cleavage present in tourmaline [10-10], which has been reported by Hawthorne and Dirlam (2011).

There is only one comprehensive study of the major-element chemistry of tourmaline from porphyry systems: Baksheev et al. (2012) showed that for the most part, the tourmaline that is present belongs to the schorl–dravite series (Fe^{2+} -Mg substitution), with a strong oxy-dravite–povondraite trend overprint. Both trends are observed in our study. As identified by our research, the alkali/alkaline-earth site can be used to help identify non-porphyry tourmaline because porphyry-related tourmaline almost exclusively contains greater than 0.5 *apfu* Na; however, major elements alone cannot definitively distinguish porphyry copper-related tourmaline from tourmaline that has formed in other geological settings.

In general, the application of LA-ICP-MS in the characterization of tourmaline is in its infancy and important issues still need to be resolved, including the complex nature and

wide chemical variation of tourmaline, paired with the difficulty of developing appropriate reference materials and internal element standards. This study has demonstrated that high-quality tourmaline trace-element data can be obtained by LA-ICP-MS. Data from the existing literature show that there are wide variations in the trace-element composition of tourmaline found in differing geological environments (Slack et al., 1999; Novak et al., 2011; Marschall et al., 2013; Hazarika et al., 2015; Kalliomäki et al., 2017). A detailed understanding of what trace elements are present, the ranges in their concentrations, and their internal relationships to other trace elements and textures are all key to understanding the provenance of tourmaline in the surficial environment. Before interpreting tourmaline trace-element data, the intrinsic and extrinsic controls on tourmaline crystal chemistry must be understood and considered. Intrinsic, or crystal-chemical, controls include ideal site size, ionic radius, and valence; extrinsic controls relate to the roles that the geological environment of formation play in affecting elemental incorporation. A summary of trace-element generalizations for tourmaline from a variety of environments is listed in Table 6. Trace elements, including Li, transition metals, reduction-oxidation (redox)–sensitive elements (Mn, As, Sn, Sb?), high field-strength elements, large-ion lithophile elements, and REEs, can be useful for characterizing tourmaline from specific environments and distinguishing it from others. Tourmaline from the Casino and Woodjam porphyry systems, as well as others examined in this study—Schaft Creek (British Columbia), Highland Valley Copper (British Columbia), Soledad (Peru), and Red Spring (British

Columbia—generally contain low concentrations of Li (<20 ppm), high concentrations of redox-sensitive elements such as Mn (av. 194 ppm) and As (av. 31.8 ppm), enrichments of Sr (av. 280 ppm), and low concentrations of Pb (<10 ppm), and have light REE–enriched patterns despite having low REE concentrations (<10 ppm Σ REE).

To explore and better explain the trace-element concentrations observed in our study, data from the literature and our data are compiled and presented as box-and-whisker plots (Fig. 9). Figure 9 shows that tourmaline from mineralized geological settings (i.e. orogenic Au, Sn-W, and porphyry deposits) contains relatively high concentrations of Cr, Co, and Ni (tens to hundreds of parts per million) and lower concentrations of Mn, Zn, and Ga relative to tourmaline forming in unmineralized environments. Specifically, tourmaline from porphyry deposits is characterized by high V (hundreds of parts per million), Cu (tens of parts per million), and Sr (hundreds of parts per million) and low Zn (tens of parts per million) and Pb (<10 ppm). Figure 10 shows the contrast of Pb–Zn composition between surficial and bedrock samples in this study and highlights the predominance of non-porphyry tourmaline in the surficial environment. Low concentrations of Pb and Zn also appear to be characteristic of tourmaline derived from surficial sediments. Although Figure 10 only shows data for Casino and Woodjam samples, the other porphyry deposit samples plot in the same Pb–Zn compositional space.

Table 6: Generalizations of trace-element composition for tourmaline from different geological settings

Deposit type	Key trace-element signatures	References
Granite	Low Sr (<25 ppm) High Ga (hundreds of parts per million) Sn (tens of parts per million)	This study – Seagull batholith
Pegmatite	Enriched in REEs, primarily LREEs High Sn (>50 ppm), high Zn (hundreds of parts per million) Commonly contain Li and Be above LOD	Novak et al. (2011); Marks et al. (2013); Hazarika et al. (2017)
Orogenic	Variable Li (tens to hundreds of parts per million) Sr (thousands of parts per million) Transition metals (twenties to hundreds of Cr, Co, Ni)	Kalliomäki et al. (2017)
Volcanogenic massive sulfide	Low Ni (<5 ppm) Variable Zn (hundreds to thousands of parts per million) Enriched in Pb (>10 ppm)	Slack et al. (1999)
Porphyry	< LOD light elements (Li and Be) Redox-sensitive elements (>50 ppm Mn) Low Zn (tens of parts per million) Sr concentrations ~hundreds of parts per million LREE enriched but low total REE to < LOD concentrations	This study
W-Sn	Low Sr (tens of parts per million) High Zn (hundreds of parts per million) High Sn (10 ppm)	Launay et al. (2018)
LOD: Limit of detection; LREE: light rare-earth elements; REE: rare-earth elements		

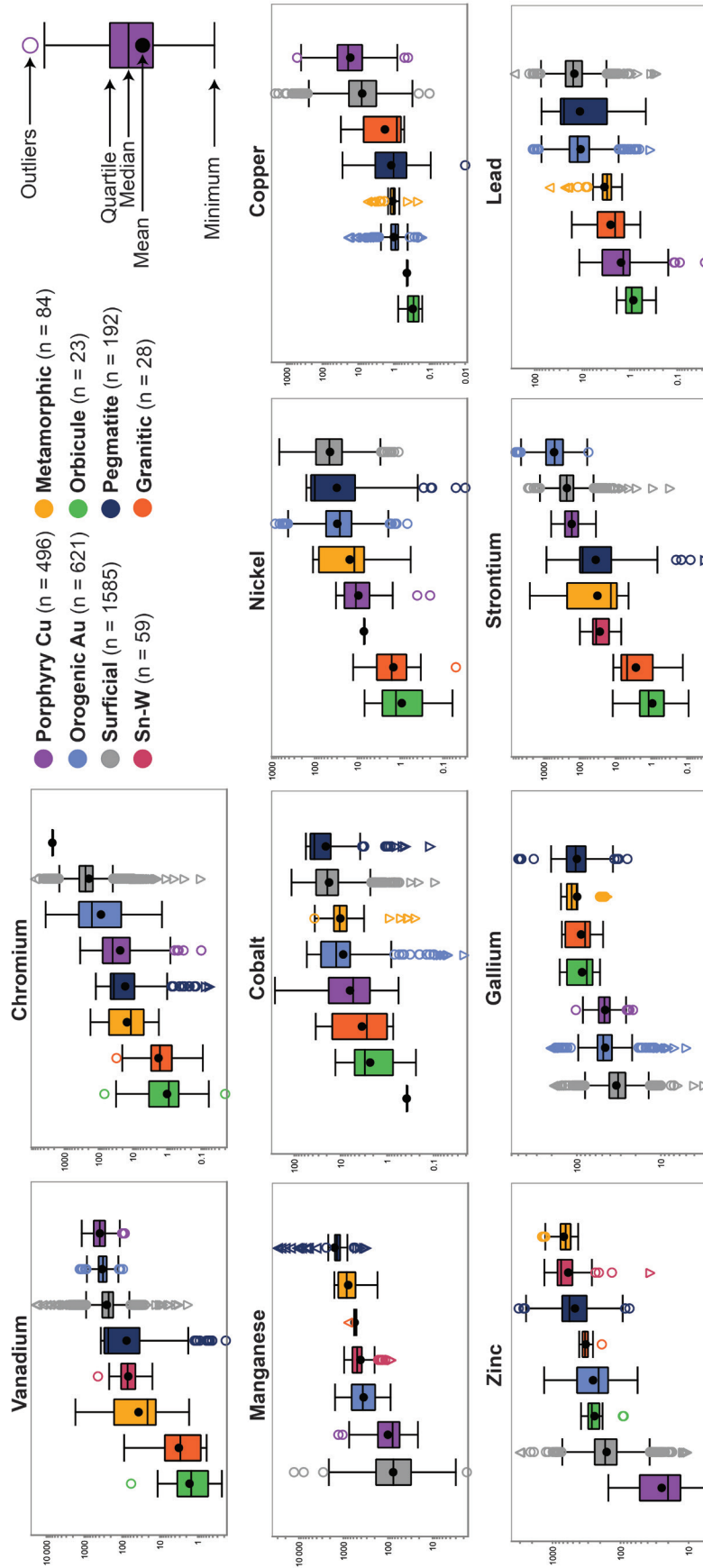


Figure 9. Tourmaline trace-element composition determined by laser-ablation inductively coupled plasma mass spectrometry for bedrock samples from the Casino and Woodjam deposits plotted as box and whisker plots and compared to data from other geological settings (Čopíková et al., 2015; Kalliomäki et al., 2017; Launay et al., 2018; Trumbull et al., 2019; Zhao et al., 2019). The term 'orbicule' refers to orbicular tourmaline granites (e.g. Sinclair and Richardson, 1992); grains classified as orogenic gold, from Finland (Kalliomäki et al., 2017); grains classified as Sn-W, from the Panasqueira deposit, Portugal (Launay et al., 2018); grains classified as 'metamorphic', from a gneiss from Vondor Falls, Ontario and represent background unmineralized bedrock (this study); and grains classified as granitic are from the Seagull batholith, Yukon and represent background unmineralized bedrock (this study). Due to the lack of published data, not all groups are plotted for all elements (e.g. Mn, Ga, and Pb).

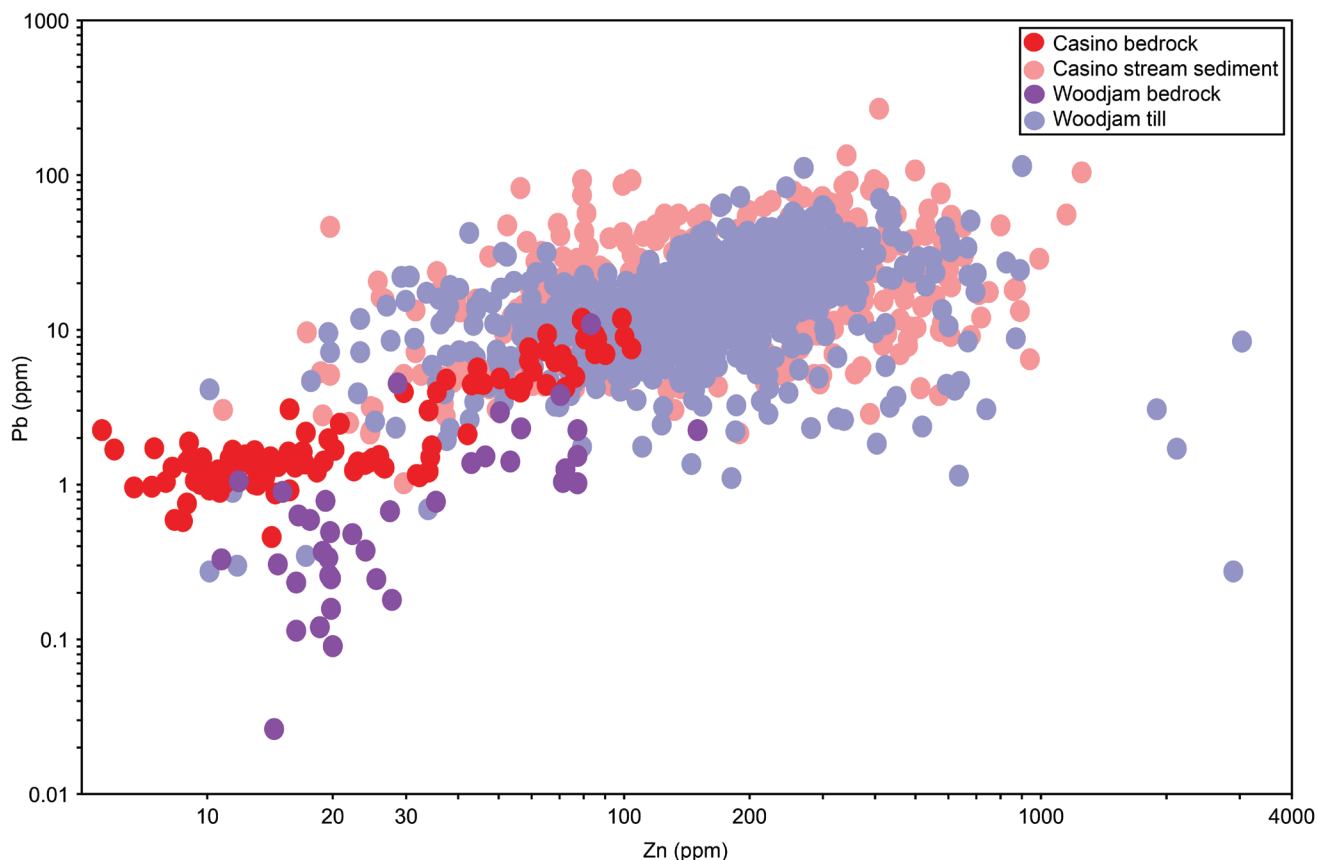


Figure 10. A Pb-Zn correlation diagram highlighting the variability of the composition of detrital tourmaline samples compared to the bedrock tourmaline from the Casino and Woodjam deposits; $n = 1930$.

The recovery of tourmaline grains from the surficial sediments around the Woodjam and Casino deposits provide an opportunity to apply our understanding of bedrock tourmaline to tourmaline of unknown origin. We classified tourmaline grains from surficial sediment samples using the physical and chemical criteria presented here. Some of the tourmaline grains in surficial sediment samples have trace-element chemical compositions consistent with those formed in porphyry deposits (Fig. 9). Based on the observed trace-element patterns and inclusion populations, greater than 90% of the tourmaline grains in the surficial sediments were likely not derived from nearby porphyry deposits. The bulk of the surficial grains, especially in till samples around the Woodjam deposit, are likely of metamorphic origin based on their physical (colour and inclusion populations) and trace-element (low Sr (tens of parts per million), hundreds of parts per million Zn, and >5000 ppm Ti) characteristics. Only 10%, likely less, of the grains in the surficial samples exhibit characteristics of tourmaline from the Woodjam cluster (Fig. 11a). The small proportion of tourmaline grains that have a composition similar to porphyry-derived grains may be due to tourmaline occurring at low concentrations in porphyry systems. For example, till samples from Woodjam typically collected from above the underlying deposit contain

less than 5% porphyry-derived tourmaline, except for two samples: one sample from the immediate deposit contains 43% porphyry-derived tourmaline and a second one, collected 11 km west-southwest (down-ice) from Takom South, the nearest known mineralized zone, contains 7% porphyry-derived tourmaline. At the Casino deposit the results are less clear (Fig. 11b). A large number of tourmaline grains from samples collected downstream of the deposit in Canadian Creek, which drains the north side of the deposit, have been classified as porphyry-derived tourmaline. In contrast, tourmaline grains from Casino Creek, on the south side of the deposit, did not display the porphyry chemical signature.

There are other factors to consider, including the colour and size of the analyzed tourmaline grains. Grain size is a challenge because much of the tourmaline observed in porphyry deposits is less than 0.25 mm or contains fractures. Despite having high hardness, tourmaline lacks distinct cleavage and is relatively brittle. This means that what is recovered from surficial sediments will undoubtedly be fragments of larger grains. As transportation distance away from the bedrock source increases, tourmaline grain size will decrease due to breakage along fractures. In some of the bedrock samples, tourmaline is acicular, with some grains

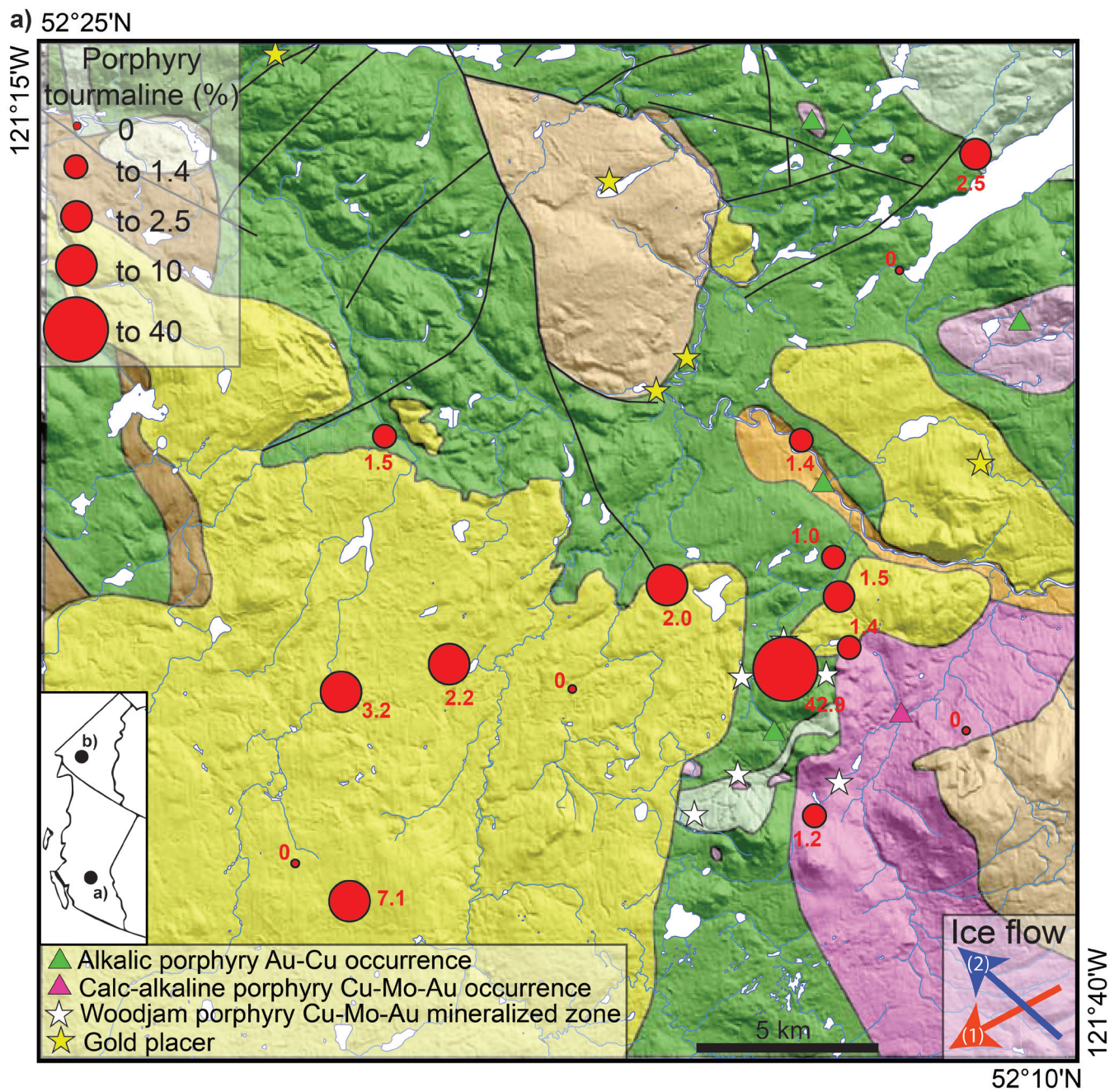


Figure 11. Percentage of tourmaline grains in each till sample identified as being derived from mineralized porphyry bedrock using criteria established in this study (lack of inclusions, high Sr concentration, and low Zn and Pb concentrations); red numbers are individual sample values. Inset map shows the location of a) the Woodjam deposit in British Columbia and b) the Casino deposit in Yukon. a) Woodjam deposit, see Plouffe and Ferbey (2017) for bedrock geology.

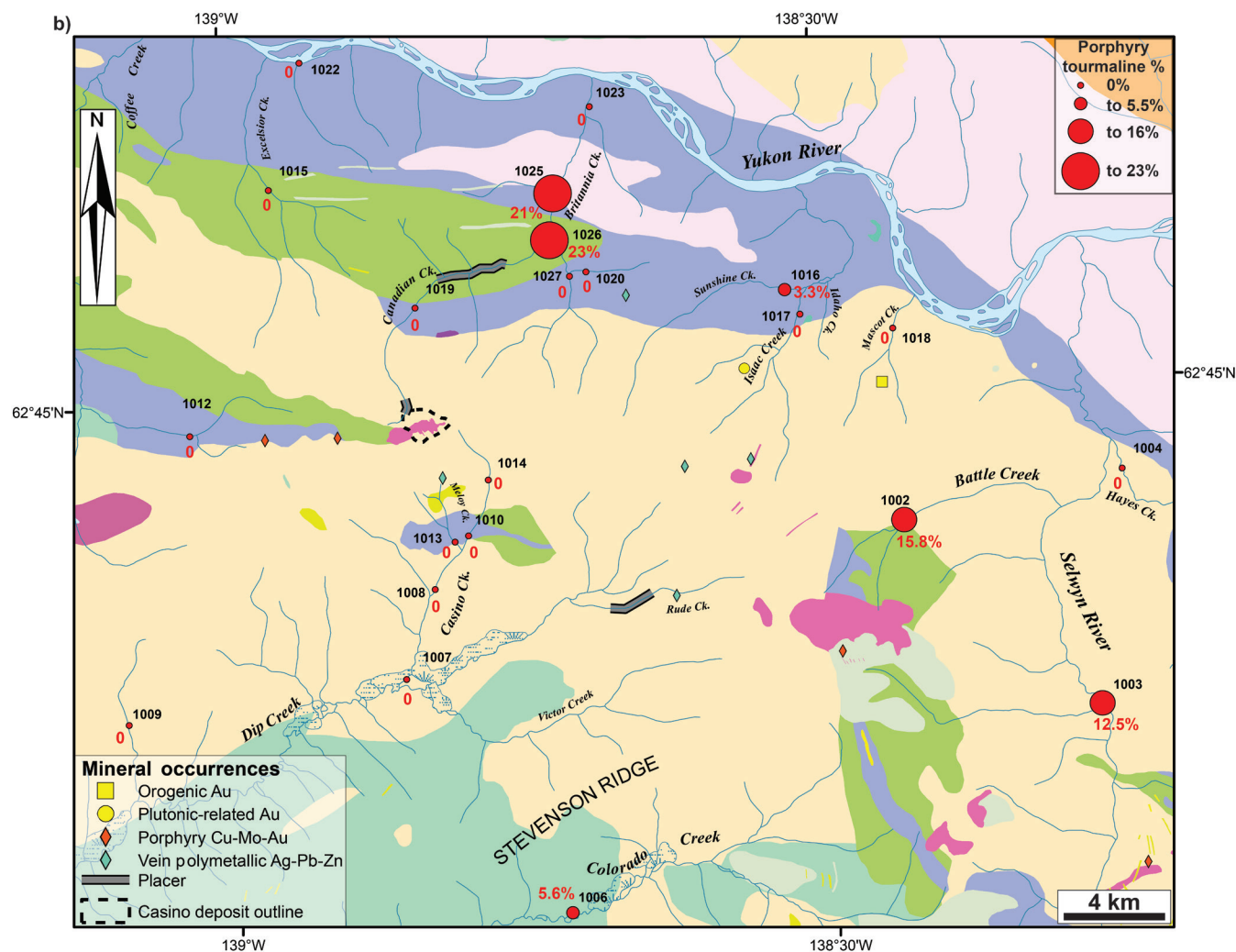


Figure 11. (cont.) b) Casino deposit, see McClenaghan et al. (2020, this volume) for bedrock geology.

being approximately 1 μm in diameter. This very small tourmaline would not be recovered in the greater than 0.25 mm fraction of sediment samples.

Colour is also a challenge. Nearly all of the tourmaline grains picked from sediment samples were black to dark brown. The lighter coloured to clear tourmaline found in the porphyry bedrock samples at Casino and Woodjam was not identified in any of the stream-sediment samples. These lighter coloured tourmaline grains may not be recovered during routine visual examinations of the greater than 0.25 mm mid-density or heavy mineral fractions of the sediment samples, possibly due to being mistaken for similarly coloured minerals, such as amphibole or epidote.

CONCLUSIONS

The physical characteristics of tourmaline (e.g. colour, grain size, morphology, colour in PPL) can assist in the classification of environment of formation. One physical characteristic that has proven useful is identifying inclusion populations (type and texture), specifically within the tourmaline grains recovered in the surficial environment.

Internal chemical zonation textures can provide information about variations in P-T-X conditions during growth. Several types of chemical zonation have been observed in tourmaline from mineralized porphyry systems and are divided between primary and secondary origins. Most important for identifying tourmaline formed in hydrothermal deposits, including tourmaline from mineralized porphyry systems, is the presence of patchy/irregular zonation,

which can reflect recrystallization, dissolution reprecipitation, and even diffusion, all features commonly observed in ore-related settings.

Although tourmaline major-element chemistry is commonly reported, it has not been demonstrated to be a definitive tool for discriminating between tourmaline from mineralized and unmineralized settings. Some generalizations about porphyry copper-related tourmaline can be made: it generally plots in the schorl–dravite classification; it follows the oxy-dravite–povondraite trend, and in general, it does not contain large quantities of Li and the X-site is always $\text{Na} > \text{Ca} > \text{K} > \square$.

There is a general paucity of trace-element data for tourmaline in the literature and even more so for tourmaline from porphyry systems. In this study, we have generated a comprehensive database of trace-element data, principally focused on tourmaline from porphyry deposits, but also including data for tourmaline from other mineralized and barren geological environments. These data will be published in a subsequent paper. We have demonstrated that the presence of a combination of V, Cu, Sr, Pb, and Zn and their relative proportions can be useful in recognizing tourmaline from porphyry deposits.

Results from this study also show that recognizing tourmaline grains in sediment samples that are from a mineralized porphyry system can be challenging, even if the sediments are proximal to a deposit. For example, at the Woodjam deposit, porphyry-related tourmaline in the surficial environment accounts for less than 5% of the total tourmaline content, except for one sample located near mineralization (47% porphyry tourmaline) and a second sample located 11 km down-ice from mineralization (7% porphyry tourmaline). Up to 23% porphyry tourmaline was identified in stream sediments in the Casino area, but only in samples from the northern drainage system. The bulk of the brown to black tourmaline recovered from the sediment samples at both study sites appears to be of metamorphic origin. The small size (<0.25 mm) and fractured nature of the tourmaline associated with porphyry mineralization could be limiting factors for its recovery in detrital sediments.

FUTURE WORK

This research is part of a larger TGI-5 project to assess the indicator mineral potential of tourmaline. Samples of tourmaline from porphyry deposits around the world are being examined to create a baseline data set for porphyry-related tourmaline compositions.

Mineral liberation analyses are planned for the 0.25 to 0.5 mm size fraction of the surficial sediment mineral concentrate samples to determine if colour bias during visual grain picking is a factor in the low percentage of porphyry tourmaline grains in the samples.

Statistical analyses of chemical and physical observations will be used to investigate whether any unique populations exist. Such data analyses will be of further aid in distinguishing porphyry-related tourmaline from other environments.

A tourmaline trace-element chemistry discrimination plot will be developed to identify grains from mineralized porphyry systems versus other mineralized or unmineralized rocks. This plot will be tested using bedrock samples and surficial sediment grains.

To investigate fluid sources of the tourmaline examined in bedrock, B, Pb, and Sr isotope analyses will be carried out to increase understanding of the relationship between tourmaline and the porphyry system.

ACKNOWLEDGMENTS

This study was funded by the Geological Survey of Canada's Targeted Geoscience Initiative (2016–2020) program and the Government of Canada's Research Affiliate Program. We are grateful for the support of Western Copper and Gold Corporation and the Casino Mining Corporation. The following companies provided sample material to this study: Chakana Copper Corp., Teck Resources Limited, New Gold Inc., Jaxton Mining Inc., Gold Fields Limited (now owned by Consolidated Woodjam Copper Corp.), Triumph Gold Corp., and Kenorland Minerals. We thank Scott Casselman (Yukon Geological Survey) for providing geological information, advice, and access to samples from deposits in Yukon and John Chapman, Martin McCurdy, and Dave Sinclair (Geological Survey of Canada) for their contributions. The manuscript was greatly improved by the reviews of L. Groat and D. Wade.

REFERENCES

- Averill, S.A., 2011. Viable indicator minerals in surficial sediments for two major base metal deposit types: Ni-Cu-PGE and porphyry Cu; *Geochemistry: Exploration, Environment, Analysis*, v. 11, no. 4, p. 279–291. <https://doi.org/10.1144/1467-7873/10-IM-022>
- Baksheev, I.A., Chitalin, A.F., Yapaskurt, V.O., Vigasina, M.F., Bryzgalov, I.A., and Ustinov, V.I., 2010. Tourmaline in the Vetka porphyry copper-molybdenum deposit of the Chukchi Peninsula of Russia; *Moscow University Geology Bulletin*, v. 65, p. 27–38. <https://doi.org/10.3103/S0145875210010035>
- Baksheev, I.A., Prokof'ev, V.Y., Yapaskurt, V.O., Vigasina, M.F., Zorina, L.D., and Solov'ev, V.N., 2011. Ferric-iron-rich tourmaline from the Darasun gold deposit, Transbaikalia, Russia; *The Canadian Mineralogist*, v. 49, no. 1, p. 263–276. <https://doi.org/10.3749/canmin.49.1.263>

- Bakshiev, I.A., Prokof'ev, V.Y., Zaraisky, G.P., Chitalin, A.F., Yapaskurt, V.O., Nikolaev, Y.N., Tikhomirov, P.L., Nagornaya, E.V., Rogacheva, L.I., Gorelikova, N.V., and Kononov, O.V., 2012. Tourmaline as a prospecting guide for the porphyry-style deposits; *European Journal of Mineralogy*, v. 24, no. 6, p. 957–979. <https://doi.org/10.1127/0935-1221/2012/0024-2241>
- Beckett-Brown, C.E., McDonald, A.M., and McClenaghan, M.B., 2019. Unravelling tourmaline in mineralized porphyry systems: assessment as a valid indicator mineral; *in* Targeted Geoscience Initiative: 2018 report of activities, (ed.) N. Rogers; Geological Survey of Canada, Open File 8549, p. 345–351. <https://doi.org/10.4095/313669>
- Bond, J.D. and Lipovsky, P.S., 2011. Surficial geology, soils and permafrost of the northern Dawson Range; *in* Yukon Exploration and Geology 2010, (ed.) K.E. MacFarlane, L.H. Weston, and C. Relf; Yukon Geological Survey, p. 19–32.
- Bouzari, F., Hart, C.J.R., Bissig, T., and Barker, S., 2016. Hydrothermal alteration revealed by apatite luminescence and chemistry: a potential indicator mineral for exploring covered porphyry copper deposits; *Economic Geology*, v. 111, no. 6, p. 1397–1410. <https://doi.org/10.2113/econgeo.111.6.1397>
- Büttner, S.H. and Kasemann, S.A., 2007. Deformation-controlled cation diffusion in tourmaline: a microanalytical study on trace elements and boron isotopes; *American Mineralogist*, v. 92, no. 11–12, p. 1862–1874. <https://doi.org/10.2138/am.2007.2567>
- Canil, D., Pisiak, L., Lacourse, T., Plouffe, A., Ferbey, T., and Grondahl, C., 2017. Magnetite as an indicator mineral in porphyry Cu±Au±Mo deposits of British Columbia, Canada; *in* Indicator minerals in till and stream sediments of the Canadian Cordillera, (ed.) T. Ferbey, A. Plouffe, and A.S. Hickin; Geological Association of Canada, Special Paper, v. 50 and Mineralogical Association of Canada, Topics in Mineral Sciences v. 47, p. 161–174.
- Casselmann, S.C. and Brown, H., 2017. Casino porphyry copper-gold-molybdenum deposit, central Yukon (Yukon MINFILE 115J028); *in* Yukon Exploration and Geology Overview 2016, (ed.) K.W. MacFarlane; Yukon Geological Survey, p. 61–74, plus digital appendices.
- Chapman, J.B., Plouffe, A., and Ferbey, T., 2015. Tourmaline: the universal indicator?; *in* Application of indicator mineral methods to exploration; Association of Applied Geochemists, 27th International Applied Geochemistry Symposium, Short Course No. 2, p. 25–31.
- Clague, J.J., and Ward, B.W., 2011. Pleistocene glaciation of British Columbia; Chapter 44 *in* Quaternary glaciations – extent and chronology – a closer look, (ed.) J. Ehlers, P.L. Gibbard, and P.D. Hughes; Developments in Quaternary Sciences, v. 15, p. 563–573. <https://doi.org/10.1016/B978-0-444-53447-7.00044-1>
- Codeço, M.S., Weis, P., Trumbull, R.B., Pinto, F., Lecumberri-Sanchez, P., and Wilke, F.D.H., 2017. Chemical and boron isotopic composition of hydrothermal tourmaline from the Panasqueira W-Sn-Cu deposit, Portugal; *Chemical Geology*, v. 468, p. 1–16. <https://doi.org/10.1016/j.chemgeo.2017.07.011>
- Codeço, M.S., Weis, P., Trumbull, R.B., Glodny, J., Wiedenbeck, M., and Romer, R.L., 2019. Boron isotope muscovite-tourmaline geothermometry indicates fluid cooling during magmatic-hydrothermal W-Sn ore formation; *Economic Geology*, v. 114, no. 1, p. 153–163. <https://doi.org/10.5382/econgeo.2019.4625>
- Cooke, D.R., Baker, M., Hollings, P., Sweet, G., Chang, Z., Danyushevsky, L.D., Gilbert, S., Zhou, T., White, N.C., Gemmell, J.B., and Inglis, S.I., 2014. New advances in detecting the distal geochemical footprints of porphyry systems – epidote mineral chemistry as a tool for vectoring and fertility assessments; Paper 7 *in* Building exploration capability for the 21st century, (ed.) K.D. Kelley and H.C. Golden; Society of Economic Geologists Special Publication 18, p. 127–152.
- Cooke, D.R., Agnew, P., Hollings, P., Baker, M., Chang, Z., Wilkinson, J.J., White, N.C., Zhang, L., Thompson, J., Gemmell, J.B., Fox, N., Chen, H., and Wilkinson, C.C., 2017. Porphyry indicator minerals (PIMS) and porphyry vectoring and fertility tools (PVFTS) – indicators of mineralization styles and recorders of hypogene geochemical dispersion haloes; *in* Proceedings of Exploration '17: Sixth Decennial International Conference on Mineral Exploration, (ed.) V. Tschirhart and M.D. Thomas; p. 457–470.
- Čopjaková, R., Škoda, R., Galiová, M.V., Novák, M., and Cempírek, J., 2015. Sc- and REE-rich tourmaline replaced by Sc-rich REE-bearing epidote-group mineral from the mixed (NYF+LCT) Kracovice pegmatite (Moldanubian Zone, Czech Republic); *American Mineralogist*, v. 100, no. 7, p. 1434–1451. <https://doi.org/10.2138/am-2015-4863>
- Dare, S.A.S., Barnes, S.J., Beaudoin, G., Méric, J., Botroy, E., and Potvin-Doucet, C., 2014. Trace elements in magnetite as petrogenetic indicators; *Mineralium Deposita*, v. 49, no. 7, p. 785–796. <https://doi.org/10.1007/s00126-014-0529-0>
- del Real, I., Bouzari, F., Rainbow, A., Bissig, T., Blackwell, J., Sherlock, R., Thompson, J.F.H., and Hart, C.R.J., 2017. Spatially and temporally associated porphyry deposits with distinct Cu/Au/Mo ratios, Woodjam district, Central British Columbia; *Economic Geology*, v. 112, no. 7, p. 1673–1717. <https://doi.org/10.5382/econgeo.2017.4526>
- Desbois, G. and Ingrin, J., 2007. Anisotropy of hydrogen diffusion in tourmaline; *Geochimica et Cosmochimica Acta*, v. 71, no. 21, p. 5233–5243. <https://doi.org/10.1016/j.gca.2007.08.027>
- Dutrow, B.L. and Henry, D.J., 2011. Tourmaline: a geologic DVD; *Elements*, v. 7, no. 5, p. 301–306.
- Dutrow, B.L. and Henry, D.J., 2017. Fibrous tourmaline: a sensitive probe of fluid compositions and petrologic environments; *The Canadian Mineralogist*, v. 54, no. 1, p. 311–335. <https://doi.org/10.3749/canmin.1600019>
- Frikken, P.H., Cooke, D.R., Walshe, J.L., Archibald, D., Skarmeta, J., Serrano, L., and Vargas, R., 2005. Mineralogical and isotopic zonation in the Sur-Sur tourmaline breccia, Rio Blanco–Los Bronces Cu-Mo deposit, Chile: implications for ore genesis; *Economic Geology*, v. 100, no. 5, p. 935–961. <https://doi.org/10.2113/100.5.935>

- Galbraith, C.G., Clarke, D.B., Trumbull, R.B., and Wiedenbeck, M., 2009. Assessment of tourmaline compositions as an indicator of emerald mineralization at the Tsa da Glisza Prospect, Yukon Territory, Canada; *Economic Geology*, v. 104, no. 5, p. 713–731. <https://doi.org/10.2113/gsecongeo.104.5.713>
- Godwin, C.I., 1976. Casino; in *Porphyry deposits of the Canadian Cordillera*, (ed.) A. Sutherland Brown; Canadian Institute of Mining and Metallurgy, Special Volume 15, p. 344–358.
- Griffin, W.L., Slack, J.F., Ramsden, A.R., Win, T.T., and Ryan, C.G., 1996. Trace elements in tourmalines from massive sulfide deposits and tourmalinites; geochemical controls and exploration application; *Economic Geology*, v. 91, no. 4, p. 657–675. <https://doi.org/10.2113/gsecongeo.91.4.657>
- Hazarika, P., Mishra, B., and Kamal Lochan, P., 2015. Diverse tourmaline compositions from orogenic gold deposits in the Hutti-Maski greenstone belt, India: implications for sources of ore-forming fluids; *Economic Geology*, v. 110, no. 2, p. 337–353. <https://doi.org/10.2113/econgeo.110.2.337>
- Hashmi, S., Ward, B.C., Plouffe, A., Leybourne, M.I., and Ferbey, T., 2015. Geochemical and mineralogical dispersal in till from the Mount Polley Cu-Au porphyry deposit, central British Columbia, Canada; *Geochemistry: Exploration, Environment, Analysis*, v. 15, no. 2, p. 234–249. <https://doi.org/10.1144/geochem2014-310>
- Hawthorne, F.C. and Dirlam, D.M., 2011. Tourmaline the indicator mineral: from atomic arrangement to Viking navigation; *Elements*, v. 7, no. 5, p. 307–312.
- Henry, D.J. and Dutrow, B.L., 1996. Metamorphic tourmaline and its petrogenetic applications; in *Boron: mineralogy, petrology and geochemistry*, (ed.) E.S. Grew and L.M. Anovitz; *Reviews in Mineralogy*, v. 33, p. 503–557.
- Henry, D.J. and Guidotti, C.V., 1985. Tourmaline as a petrogenetic indicator mineral: an example from the staurolite-grade metapelites of NW Maine; *American Mineralogist*, v. 70, no. 1–2, p. 1–15.
- Jochum, K.P., Weis, U., Stoll, B., Kuzmin, D., Yang, Q., Raczek, I., Jacob, D.E., Stracke, A., Birbaum, K., Frick, D.A., Günther, D., and Enzweiler, J., 2011. Determination of reference values for NIST SRM 610–617 glasses following ISO guidelines; *Geostandards and Geoanalytical Research*, v. 35, no. 4, p. 397–429. <https://doi.org/10.1111/j.1751-908X.2011.00120.x>
- Kalliomiäki, H., Wagner, T., Fusswinkel, T., and Sakellaris, G., 2017. Major and trace element geochemistry of tourmalines from Archean orogenic gold deposits: proxies for the origin of gold mineralizing fluids?; *Ore Geology Reviews*, v. 91, p. 906–927. <https://doi.org/10.1016/j.oregeorev.2017.08.014>
- Kelley, K.D., Eppinger, R.G., Lang, J., Smith, S.M., and Fey, D.L., 2011. Porphyry Cu indicator minerals in till as an exploration tool: example from the giant Pebble porphyry Cu-Au-Mo deposit, Alaska, USA; *Geochemistry: Exploration, Environment, Analysis*, v. 11, no. 4, p. 321–334. <https://doi.org/10.1144/1467-7873/10-IM-041>
- Launay, G., Sizaret, S., Guillou-Frottier, L., Gloaguen, E., and Pinto, F., 2018. Deciphering fluid flow at the magmatic-hydrothermal transition: a case study from the world-class Panasqueira W-Sn-(Cu) ore deposit (Portugal); *Earth and Planetary Science Letters*, v. 499, p. 1–12. <https://doi.org/10.1016/j.epsl.2018.07.012>
- Lu, Y.-J., Loucks, R.R., Fiorentini, M., McCuaig, T.C., Evans, N.J., Yang, Z.-M., Hou, Z.-Q., Kirkland, C.L., Parra-Avila, L.A., and Kobussen, A., 2016. Zircon compositions as a pathfinder for porphyry Cu±Mo±Au deposits; in *Tectonics and metallogeny of the Tethyan orogenic belt*, (ed.) J.P. Richards; *Society of Economic Geologists, Special Publication 19*, p. 329–347.
- Manégliá, N., Beaudoin, G., and Simard, M., 2018. Indicator minerals of the Meliadine orogenic gold deposits, Nunavut (Canada), and application to till surveys; *Geochemistry: Exploration, Environment, Analysis*, v. 18, no. 3, p. 241–251. <https://doi.org/10.1144/geochem2017-036>
- Mao, M., Rukhlov, A.S., Rowins, S.M., Spence, J., and Coogan, L.A., 2016. Apatite trace element compositions: a robust new tool for mineral exploration; *Economic Geology*, v. 111, no. 5, p. 1187–1222. <https://doi.org/10.2113/econgeo.111.5.1187>
- Marks, M.A.W., Marschall, H.R., Schuhle, P., Guth, A., Wenzel, T., Jacob, D.E., Barth, M., and Markl, G., 2013. Trace element systematics of tourmaline in pegmatitic and hydrothermal systems from the Variscan Schwarzwald (Germany): the importance of major element composition, sector zoning, and fluid or melt composition; *Chemical Geology*, v. 344, p. 73–90. <https://doi.org/10.1016/j.chemgeo.2013.02.025>
- Marschall, H.R. and Jiang, S.Y., 2011. Tourmaline isotopes: no element left behind; *Elements*, v. 7, no. 5, p. 313–319.
- McClenaghan, M.B., McCurdy, M.W., Beckett-Brown, C.E., and Casselman, S.C., 2020. Indicator mineral signatures of the Casino porphyry Cu-Au-Mo deposit, Yukon. *Geological Survey of Canada, Open File 8711*, 42 p. <https://doi.org/10.4095/322191>
- McCurdy, M.W., McClenaghan, M.B., Garrett, R.G., and Pelchat, P., 2019. The stream sediment geochemical signature of the Casino porphyry Cu-Au-Mo deposit, Yukon Territory: a case study; *Geological Survey of Canada, Open File 8632*, 39 p. <https://doi.org/10.4095/321381>
- Novak, M., Skoda, R., Filip, J., Macek, I., and Vaculovic, T., 2011. Compositional trends in tourmaline from intragranitic NYF pegmatites of the Trebic pluton, Czech Republic: an electron microprobe, Mossbauer and LA-ICP-MS study; *The Canadian Mineralogist*, v. 49, no. 1, p. 359–380. <https://doi.org/10.3749/canmin.49.1.359>
- Palmer, M.R., London, D., Morgan, G.B., and Babb, H.A., 1992. Experimental-determination of fractionation of B-11/B-10 between tourmaline and aqueous vapor - a temperature-dependent and pressure-dependent isotopic system; *Chemical Geology*, v. 101, no. 1–2, p. 123–129. [https://doi.org/10.1016/0009-2541\(92\)90209-N](https://doi.org/10.1016/0009-2541(92)90209-N)
- Paton, C., Hellstrom, J., Paul, B., Woodhead, J., and Hergt, J., 2011. Iolite: freeware for the visualisation and processing of mass spectrometric data; *Journal of Analytical Atomic Spectrometry*, v. 26, no. 12, p. 2508–2518. <https://doi.org/10.1039/C1JA10172B>

- Pisiak, L., Canil, D., Lacourse, T., Plouffe, A., and Ferbey, T., 2017. Magnetite as an indicator mineral in the exploration of porphyry deposits: a case study in till near the Mount Polley Cu-Au deposit, British Columbia, Canada; *Economic Geology*, v. 112, no. 4, p. 919–940. <https://doi.org/10.2113/econgeo.112.4.919>
- Plouffe, A. and Ferbey, T., 2016. Till geochemistry, mineralogy and textural data near four Cu porphyry deposits in British Columbia; Geological Survey of Canada, Open File 8038, 44 p. and British Columbia Ministry of Energy and Mines, British Columbia Geological Survey, Geofile 2016-10, 1 .zip file. <https://doi.org/10.4095/298805>
- Plouffe, A. and Ferbey, T., 2017. Porphyry Cu indicator minerals in till: a method to discover buried mineralization; *in* Indicator minerals in till and stream sediments of the Canadian Cordillera, (ed.) T. Ferbey, A. Plouffe, and A. Hicken; Geological Association of Canada, Special Paper, v. 50, and Mineralogical Association of Canada, Topics in Mineral Sciences, v. 47, p. 129–159.
- Plouffe, A., Ferbey, T., Hashmi, S., and Ward, B.C., 2016. Till geochemistry and mineralogy: vectoring towards Cu porphyry deposits in British Columbia, Canada; *Geochemistry: Exploration, Environment, Analysis*, v. 16, no. 3–4, p. 213–232. <https://doi.org/10.1144/geochem2015-398>
- Raczek, I., Stoll, B., Hofmann, A.W., and Jochum, K.P., 2001. High-precision trace element data for the USGS reference materials BCR-1, BCR-2, BHVO-1, BHVO-2, AGV-1, AGV-2, DTS-1, DTS-2, GSP-1 and GSP-2 by ID-TIMS and MIC-SSMS; *Geostandards and Geoanalytical Research*, v. 25, no. 1, p. 77–86. <https://doi.org/10.1111/j.1751-908X.2001.tb00789.x>
- Sillitoe, R.H., 2010. Porphyry copper systems; *Economic Geology*, v. 105, no. 1, p. 3–41. <https://doi.org/10.2113/gsecongeo.105.1.3>
- Sinclair, W.D. and Richardson, J.M., 1992. Quartz-tourmaline orbicules in the Seagull Batholith, Yukon Territory; *The Canadian Mineralogist*, v. 30, no. 3, p. 923–935.
- Slack, J.F., 1996. Tourmaline associations with hydrothermal ore deposits. Chapter 11 *in*: Boron: mineralogy, petrology and geochemistry, (ed.) E.S. Grew and L.M. Anovitz; *Reviews in Mineralogy*, v. 33, p. 559–643.
- Slack, J.F. and Coad, P.R., 1989. Multiple hydrothermal and metamorphic events in the Kidd Creek volcanogenic massive sulphide deposit, Timmins, Ontario: evidence from tourmalines and chlorites; *Canadian Journal of Earth Sciences*, v. 26, no. 4, p. 694–715. <https://doi.org/10.1139/e89-059>
- Slack, J.F. and Trumbull, R.B., 2011. Tourmaline as a recorder of ore-forming processes; *Elements*, v. 7, no. 5, p. 321–326.
- Slack, J.F., Palmer, M.R., Stevens, B.P.J., and Barnes, R.G., 1993. Origin and significance of tourmaline-rich rocks in the Broken Hill district, Australia; *Economic Geology*, v. 88, no. 3, p. 505–541. <https://doi.org/10.2113/gsecongeo.88.3.505>
- Slack, J.F., Ramsden, A.R., Griffin, W.L., Win, T.T., French, D.H., and Ryan, C.G., 1999. Trace elements in tourmaline from the Kidd Creek massive sulfide deposit and vicinity, Timmins, Ontario: a proton microprobe study; *in* The giant Kidd Creek volcanogenic massive sulfide deposit, western Abitibi Subprovince, Canada, (ed.) M.D. Hannington and C.T. Barrie; *Economic Geology Monograph*, v. 10, p. 415–430.
- Testa, F., Villanueva, C., Cooke, D., and Zhang, L., 2018. Lithological and hydrothermal alteration mapping of epithermal, porphyry and tourmaline breccia districts in the Argentine Andes using ASTER imagery; *Remote Sensing*, v. 10, no. 2, p. 203. <https://doi.org/10.3390/rs10020203>
- Trumbull, R.B., Garda, G.M., Xavier, R.P., Cavalcanti, J.A.D., and Codeço, M.S., 2019. Tourmaline in the Passagem de Mariana gold deposit (Brazil) revisited: major-element, trace-element and B-isotope constraints on metallogenesis; *Mineralium Deposita*, v. 54, no. 3, p. 395–414. <https://doi.org/10.1007/s00126-018-0819-z>
- van Hinsberg, V.J., Henry, D.J., and Marschall, H.R., 2011. Tourmaline: an ideal indicator of its host environment; *The Canadian Mineralogist*, v. 49, no. 1, p. 1–16. <https://doi.org/10.3749/canmin.49.1.1>
- Wilkinson, J.J., Cooke, D.R., Baker, M.J., Chang, Z., Wilkinson, C.C., Chen, H., Fox, N., Hollings, P., White, N.C., Gemmell, J.B., Loader, M.A., Pacey, A., Sievwright, R.H., Hart, L.A., and Brugge, E.R., 2017. Porphyry indicator minerals and their mineral chemistry as vectoring and fertility tools; *in* Application of indicator mineral methods to bedrock and sediments, (ed.) M.B. McClenaghan and D. Layton-Matthews; Geological Survey of Canada, Open File 8345, p. 67–77. <https://doi.org/10.4095/306317>
- Xu, L., Bi, X., Hu, R., Tang, Y., Wang, X., and Xu, Y., 2015. LA-ICP-MS mineral chemistry of titanite and the geological implications for exploration of porphyry Cu deposits in the Jinshajiang – Red River alkaline igneous belt, SW China; *Mineralogy and Petrology*, v. 109, no. 2, p. 181–200. <https://doi.org/10.1007/s00710-014-0359-x>
- Yavuz, F., Karakaya, N., Yıldırım, D. K., Karakaya, M.Ç., and Kumral, M., 2014. A Windows program for calculation and classification of tourmaline-supergroup (IMA-2011); *Computers & Geosciences*, v. 63, p. 70–87. <https://doi.org/10.1016/j.cageo.2013.10.012>
- Zhao, H.-D., Zhao, K.-D., Palmer, M.R., and Jiang, S.-Y., 2019. In-situ elemental and boron isotopic variations of tourmaline from the Sanfang granite, South China: insights into magmatic-hydrothermal evolution; *Chemical Geology*, v. 504, p. 190–204. <https://doi.org/10.1016/j.chemgeo.2018.11.013>

APPENDIX A

Detrital tourmaline recount data

The table containing tourmaline grain recounts from heavy mineral concentrates of till samples collected surrounding the Woodjam deposit, British Columbia is found in the file [POR-09_Appendix A.xlsx](#). This Appendix has not been edited to Geological Survey of Canada specifications. The data are listed by sample numbers. The location of the samples can be found in Plouffe and Ferbey (2016).